

# Single-cell mapping of the thymic stroma identifies IL-25-producing tuft epithelial cells

Chamutal Bornstein<sup>1,6</sup>, Shir Nevo<sup>1,6</sup>, Amir Giladi<sup>1,6</sup>, Noam Kadouri<sup>1,6</sup>, Marie Pouzolles<sup>2</sup>, François Gerbe<sup>3</sup>, Eyal David<sup>1</sup>, Alice Machado<sup>2</sup>, Anna Chuprin<sup>1</sup>, Beáta Tóth<sup>4</sup>, Ori Goldberg<sup>5</sup>, Shalev Itzkovitz<sup>4</sup>, Naomi Taylor<sup>2</sup>, Philippe Jay<sup>3</sup>, Valérie S. Zimmermann<sup>2</sup>, Jakub Abramson<sup>1,7\*</sup> & Ido Amit<sup>1,7\*</sup>

**T cell development and selection are coordinated in the thymus by a specialized niche of diverse stromal populations<sup>1–3</sup>. Although much progress has been made over the years in identifying the functions of the different cell types of the thymic stromal compartment, there is no comprehensive characterization of their diversity and heterogeneity. Here we combined massively parallel single-cell RNA-sequencing<sup>4,5</sup>, spatial mapping, chromatin profiling and gene targeting to characterize de novo the entire stromal compartment of the mouse thymus. We identified dozens of cell states, with thymic epithelial cells (TECs) showing the highest degree of heterogeneity. Our analysis highlights four major medullary TEC (mTEC I–IV) populations, with distinct molecular functions, epigenetic landscapes and lineage regulators. Specifically, mTEC IV constitutes a new and highly divergent TEC lineage with molecular characteristics of the gut chemosensory epithelial tuft cells. Mice deficient in *Pou2f3*, a master regulator of tuft cells, have complete and specific depletion of mTEC IV cells, which results in increased levels of thymus-resident type-2 innate lymphoid cells. Overall, our study provides a comprehensive characterization of the thymic stroma and identifies a new tuft-like TEC population, which is critical for shaping the immune niche in the thymus.**

The thymus constitutes a specialized lymphoid organ, where immature T lymphocytes are educated to recognize foreign antigens, while tolerating self<sup>1</sup>. The T cell ‘educational program’ involves two central steps, which occur in two anatomical compartments of the thymus, the cortex and the medulla. Both compartments are characterized by the presence of specialized stromal cells, which provide the desired microenvironment for different checkpoints in T cell development and selection<sup>2,3</sup>. Cortical thymic epithelial cells (cTEC) coordinate the early stages of T cell development and positive selection of thymocytes<sup>6</sup>. The later steps of T cell development, including negative selection, are primarily carried out by mTECs<sup>1–3</sup>.

Although much progress has been made over the years in elucidating the function of the different cell types of the thymic stroma, their diversity, heterogeneity and molecular pathways are still poorly characterized. To de novo characterize the entire stromal compartment of the thymus, we performed massively parallel single-cell RNA-sequencing (MARS-seq)<sup>4,5</sup> of 1,825 non-haematopoietic cells (CD45<sup>−</sup>) isolated from adult mouse thymi (Extended Data Fig. 1). In order to link the canonical surface markers to the single-cell RNA-sequencing data, we used an index sorting strategy that allowed for retrospective analysis of surface markers of each individual cell. We then used the MetaCell pipeline to identify homogeneous and robust groups of cells (Methods). This analysis showed that the thymic stroma is composed of three major lineages, consisting of fibroblasts (*Col1a1* and *Col6a1*), endothelial cells (*Pecam1* and *Flt1*) and epithelial cells (*Epcam* and various keratin genes; Fig. 1a–c and Extended Data Fig. 2). Of the three lineages, the epithelial cells displayed the largest heterogeneity in gene-expression programs

(Extended Data Fig. 2 and Supplementary Tables 1, 2), suggesting that they are more complex and heterogeneous than previously anticipated.

In order to comprehensively characterize the TEC compartment, we sorted additional 1,716 CD45<sup>−</sup>EpCAM<sup>+</sup> single cells (Extended Data Figs 1, 3). Clustering analysis combined with two-dimensional projection of the epithelial cells from both datasets revealed dozens of different TEC subpopulations (Fig. 1d, e, Extended Data Fig. 3 and Supplementary Table 2). The TEC subpopulations clustered within five major molecular types, each distributed at a distinct position within the two-dimensional projection (Fig. 1d and Extended Data Fig. 3). Index sorting analysis using the canonical cortical (Ly51) and medullary (UEA1) markers revealed that only one of the groups corresponds to the Ly51<sup>+</sup>UEA1<sup>−</sup> population and expresses cTEC-specific genes, including *Prss16*, *Psm11* and *Ctsl*<sup>2,3</sup>. By contrast, the other four TEC populations stained positively for UEA1 and had no or low expression of Ly51 (Extended Data Fig. 3), suggesting that these cells reside in the medulla. This was further validated by immunofluorescence staining and single-molecule RNA fluorescence in situ hybridization using a panel of markers specific to the individual TEC subpopulations (Fig. 1f and Extended Data Fig. 3). Therefore, on the basis of these data, we reclassified the mTEC compartment into four major groups (mTEC I–IV), reflecting their distinct transcriptional and molecular characteristics. Specifically, mTEC I is characterized by high expression of *Iga6* and *Sca1* (also known as *Ly6a*) (Fig. 1e and Extended Data Fig. 3), expression of which have previously been associated with putative TEC progenitors<sup>7</sup>. The mTEC II population is characterized by specific expression of the canonical markers of mature mTECs, including high expression of *Aire*, *Fzf2*, *Cd40*, *H2-Aa* or *Cd74* (Fig. 1e and Extended Data Fig. 3). mTEC III represents a heterogeneous population expressing several unique genes (*Pigr*, *Ly6d*, *Spink5*, *Ivl* and *Krt10*), some of which have been linked to a putative population of mTEC that previously expressed AIRE (post-AIRE cells)<sup>8,9</sup> (Fig. 1e and Extended Data Fig. 3). Notably, the mTEC IV population does not express any classical mTEC or cTEC markers, but rather a unique set of genes such as *Lrrmp*, *Avil*, *Trpm5*, *Dcl1*, *Gng13*, *L1cam* and *Sox9* (Fig. 1e and Extended Data Fig. 3).

To investigate the dynamics of the different TEC populations during early development, we performed MARS-seq analysis of 3,074 sorted CD45<sup>−</sup>EpCAM<sup>+</sup> single cells isolated from thymi at major developmental stages: embryonic day 14.5 (E14.5), E18.5 and day 6 after birth (Extended Data Figs. 1, 4). Because the developing thymus may have additional cell types or states that are not observed in the adult, we associated embryonic TEC metacells with adult phenotypes only if a large fraction of their cell neighbours was of adult origin (Methods, Fig. 1g, Extended Data Fig. 4 and Supplementary Table 3). This analysis highlighted the dynamic changes in the TEC compartment during thymus organogenesis. Although most of the E14.5 TECs were relatively homogenous and expressed a large number of cTEC-specific

<sup>1</sup>Department of Immunology, Weizmann Institute of Science, Rehovot, Israel. <sup>2</sup>Institut de Génétique Moléculaire de Montpellier, University of Montpellier, CNRS, Montpellier, France. <sup>3</sup>IGF, CNRS, INSERM, University of Montpellier, Montpellier, France. <sup>4</sup>Department of Cell Biology, Weizmann Institute of Science, Rehovot, Israel. <sup>5</sup>Department of Pediatrics, Schneider Children’s Medical Center, Petach Tikva, Israel. <sup>6</sup>These authors contributed equally: Chamutal Bornstein, Shir Nevo, Amir Giladi, Noam Kadouri. <sup>7</sup>These authors jointly supervised this work: Jakub Abramson, Ido Amit. \*e-mail: jakub.abramson@weizmann.ac.il; ido.amit@weizmann.ac.il

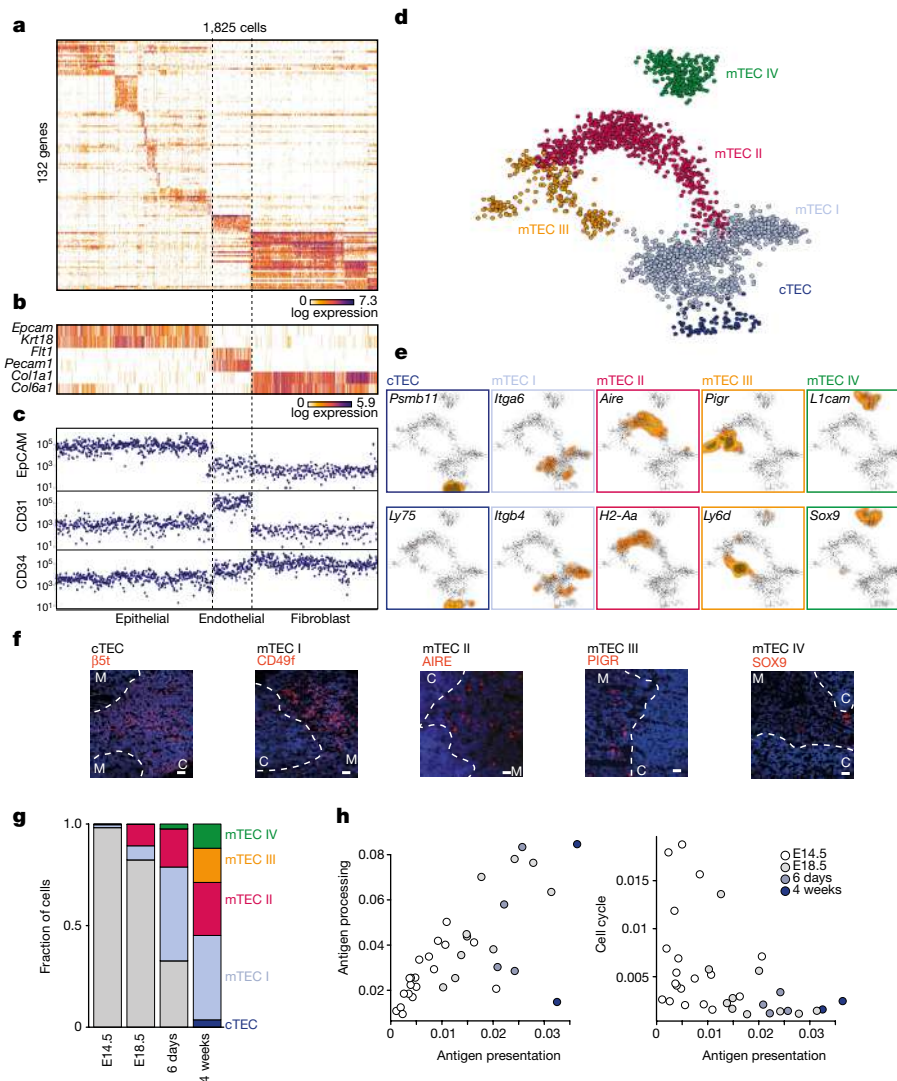


**Fig. 1 | The medulla epithelial compartment has diverse molecular functions.** **a**, Clustering analysis of 1,825 thymic stromal (CD45<sup>+</sup>) cells from seven biological replicates of 4–6-week-old mice. **b**, Expression of selected marker genes. **c**, Index sorting tracks showing protein level intensity. **d**, Two-dimensional graphical representation of 2,341 single CD45<sup>+</sup>-EpCAM<sup>+</sup> cells separated into five TEC subsets. **e**, Kernel density projection of differentially expressed genes onto the two-dimensional graph. **f**, Immunofluorescence images of thymus sections. Medulla (M) and cortex (C) are separated by a dashed line, distinguished by nuclei

genes, their general transcriptional signature was distinct from adult cTECs (Fig. 1g and Extended Data Fig. 4). Specifically, we observed progressive downregulation of cell cycle genes and upregulation of the MHC-II pathway in the adult compared to the embryonic cTECs (Fig. 1h, Extended Data Fig. 4 and Methods). While none of the adult mTEC subpopulations were present at the E14.5 stage, mTEC I and II, but not mTEC III and IV, became detectable in the thymus at E18.5 (Fig. 1g and Extended Data Fig. 4). At neonatal day 6, mTEC I, II and IV were present, although with different frequencies than in the adult thymus (Fig. 1g and Extended Data Fig. 4). Measuring the percentage of proliferating cells, we found that E14.5 TECs are the most proliferative cells in the thymus, while after birth most of the TEC proliferation is restricted to mTEC I and mTEC II cells (Extended Data Fig. 4).

To further characterize the newly defined mTEC subtypes, we established a new sorting strategy, based on a panel of surface markers unique to each population (Fig. 2a). This strategy was validated by MARS-seq and qPCR analyses of sorted EpCAM<sup>+</sup> populations, which were gated according to this scheme (Fig. 2b and Extended Data

density. Blue, DAPI.  $\beta 5t$  is also known as PSMB11; CD49f is also known as ITGA6. Scale bars, 40  $\mu$ m. Images are representative of three independent animals with similar results. **g**, Distribution of the TEC subsets along four developmental time points. Grey labels represent cells distinct from adult TECs. **h**, Progression of early cTECs towards adult cTECs. Circles represent cTEC metacells coloured by the developmental time points of the majority of cells. Axes represent share of each gene module from the entire metacell transcriptome.

Fig. 5). Profiling the putative enhancer regulatory elements (marked by H3K4me2) of the four mTEC populations using indexing-first chromatin immunoprecipitation followed by deep sequencing<sup>10</sup> revealed that each subset is characterized by a unique set of distal enhancer regions with the mTEC IV population showing the most distinct regulatory elements (Fig. 2c, d, Extended Data Fig. 5 and Extended Data Table 1). In order to determine specific transcription-factor-binding sites, we performed an assay of transposase-accessible chromatin and analysed peaks of open chromatin within enhancer regions<sup>11</sup>, followed by de novo motif finding (Extended Data Fig. 5 and Extended Data Table 1). This analysis revealed that accessible enhancer regions in mTEC II cells are significantly enriched ( $P = 10^{-109}$ ; binomial test) for a binding-motif signature of the NF- $\kappa$ B family, correlating with specific expression of the *Nfkb2* gene in mTEC II cells (Fig. 2d–f and Extended Data Fig. 5). By contrast, mTEC-IV-specific enhancers were significantly enriched ( $P = 10^{-805}$ ) for the POU class 2 transcription-factor motif, correlating with the specific expression of the *Pou2f3* gene in mTEC IV cells (Fig. 2d–f and Extended Data Fig. 5).

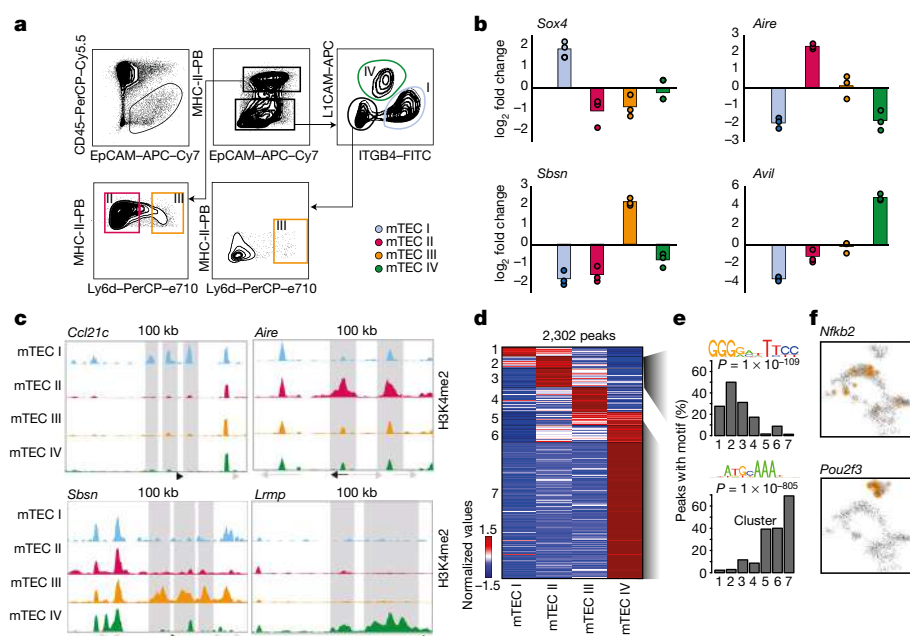


**Fig. 2 | Genetic and epigenetic characterization of TEC subsets.** **a**, Gating strategy for fluorescence-activated cell sorting to isolate mTEC subsets. **b**, qPCR analysis of mTEC subsets. Values represent fold change from the sample mean.  $n = 3$  biologically independent animals. Data are mean (bars) and individual animals (dots). **c**, Normalized H3K4me2 profiles in 100-kb regions around differential mTEC gene loci. Differential genes are specified by black arrows. Plots are representative of four animals from two independent experiments. **d**, Peak intensities of 2,302 differential peaks between the four mTEC subsets (clusters 1–7;  $K$ -means;  $K = 7$ ). **e**, Transcription-factor motif analysis showing enrichment of motifs in accessible regions within H3K4me2-marked peaks; bars indicate motif abundance in H3K4me2 peaks clusters 1–7. False-discovery rate-corrected binomial test;  $n = 137$  and 1,559 peaks. **f**, Projection of transcription factors onto the two-dimensional graph (Fig. 1).

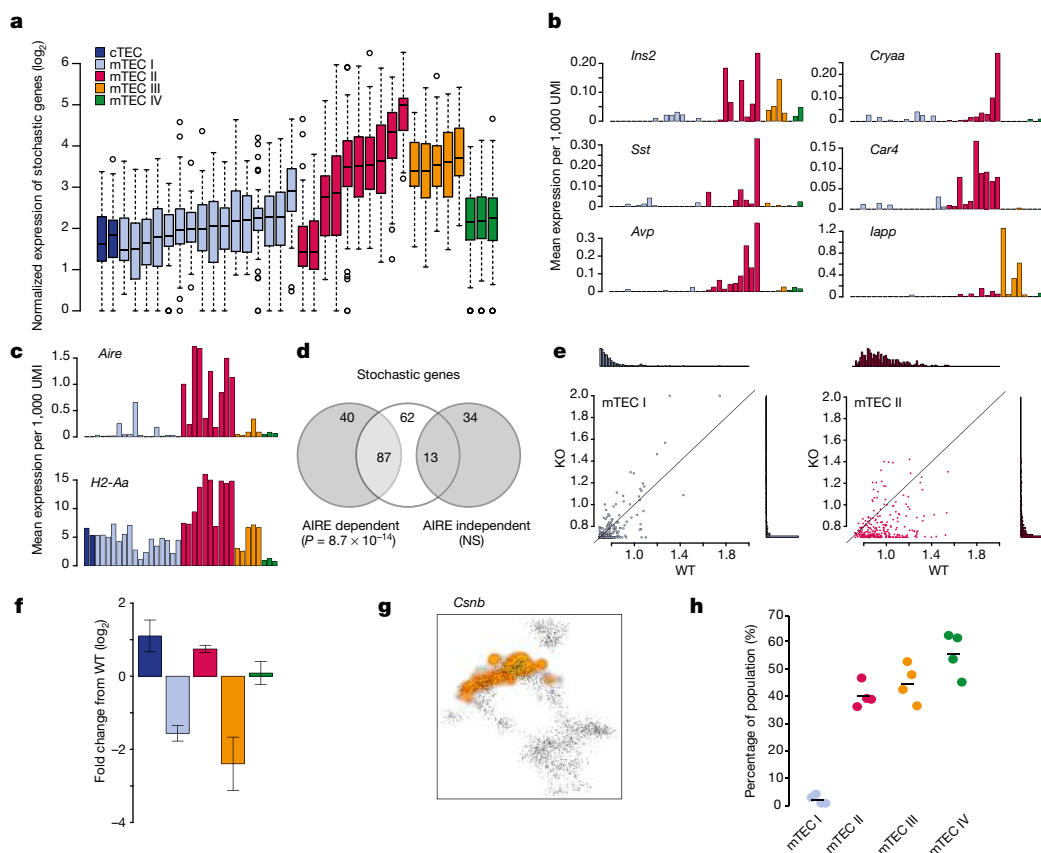


**Fig. 3 | Characterization of AIRE-dependent mTEC subsets.** **a**, Total expression distribution of stochastically expressed genes across the TEC metacells. In the box plots, bars indicate median, boxes are the first–third quantiles, whiskers, 5th–95th percentile and outlier are shown as circles.  $n = 2,341$  single cells. **b**, **c**, Mean normalized expression of representative TRA genes (**b**), *Aire* and *H2-Aa* (**c**) across TEC metacells. **d**, Venn diagram depicting overlap between stochastically expressed genes and an established list of AIRE-dependent and -independent TRA genes. Hypergeometric test.  $n = 388$  differentially expressed genes. **e**, Comparison of stochastic gene expression between *Aire* knockout

(KO) and wild-type (WT) cells in TEC subsets. Marginal distributions are shown as histograms. Axes represent UMI count per 1,000 UMI, normalized to cell numbers. **f**, Bar plots showing  $\log_2$  fold change between TEC subpopulation abundances in *Aire* knockout and wild-type mice. Error bars represent 95% confidence intervals.  $n = 1,332$  knockout and 1,638 wild-type cells. **g**, Projection of *Csnb* onto the two-dimensional graph (Fig. 1). **h**, Percentage of tdTomato-expressing cells in mTEC I–IV.  $n = 4$  biologically independent mice. Data are mean (line) and individual animals (dots).



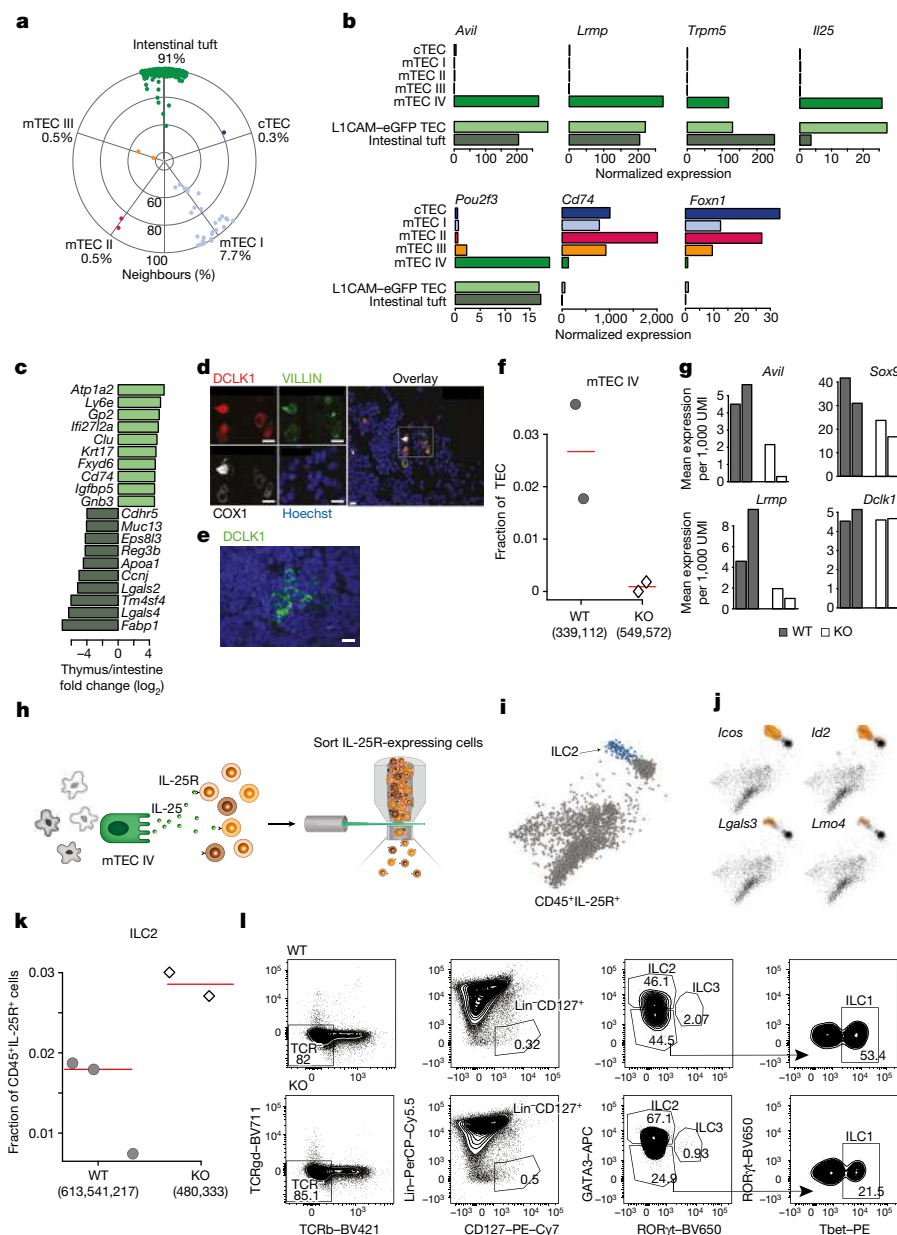


**Fig. 4 | mTEC IV, a new TEC population with tuft-cell characteristics.** **a**,  $K$ -nearest neighbours quantification ( $K=50$ ) of thymic  $L1CAM^+ Sox9-eGFP^+$  cells (mTEC IV) mapped to both TEC subsets and intestinal  $Hpgds-tdTomato^+$  tuft cells (expressing  $tdTomato$  under  $Hpgds$  promoter). Radial location signifies populations with the highest number of neighbours; y axis indicates percentage of all nearest neighbours. **b**, Normalized mean expression of differentially expressed genes across TEC subsets,  $L1CAM^+ Sox9-eGFP^+$  ( $n=376$ ) and intestinal  $Hpgds-tdTomato^+$  ( $n=1,879$  single cells) cells. **c**, Differential gene expression between  $L1CAM^+ Sox9-eGFP^+$  and intestinal  $Hpgds-tdTomato^+$  cells ( $\log_2$  fold change). **d**, **e**, Representative immunofluorescence imaging of tuft markers in thymic medulla sections from adult mice (**d**) and human tissue (**e**). Blue, DAPI. Scale bar =  $10\ \mu m$ . Images are representative of two independent experiments with similar results. **f**, Fraction of thymic mTEC IV cells from total TEC numbers in  $Pou2f3$  knockout and wild-type mice. Numbers in brackets indicate analysed cells in biological duplicates, indicated by individual circles and diamonds. Horizontal lines represent mean value. **g**, Mean expression of tuft markers in mTEC IV cells from wild-type and  $Pou2f3$  knockout mice. **h**, Experimental flow for exploring effect of mTEC IV cells on  $IL-25R^+$  immune cells. **i**, Two-dimensional graphical representation of 3,500  $CD45^+ IL-25R^+$  single cells separated into metacells. Blue dots label ILC2s. **j**, Projection of ILC2 markers onto the two-dimensional graph. **k**, Fraction of thymic ILC2 cluster from total  $CD45^+ IL-25R^+$  numbers in  $Pou2f3$  knockout and wild-type mice. Numbers in brackets indicate analysed cells in each replicate. Horizontal lines represent mean value and circles and diamonds indicate individual mice. **l**, ILC subtypes in  $Pou2f3$  knockout and wild-type thymi assessed by flow cytometry. Representative plots are shown ( $n=4$  biologically independent animals).

Given that one of the key functional roles of mTECs is to ectopically express and cross-present a plethora of tissue-restricted antigens (TRAs)<sup>1,2</sup>, we analysed the level of TRA gene expression within the TEC compartment. Because the expression of most TRAs is stochastic and AIRE-dependent<sup>12,13</sup>, we first defined a list of stochastically expressed genes in mTECs, based on their high expression variance and low correlation to other genes (Fig. 3, Extended Data Fig. 6, Supplementary Table 4 and Methods). As expected, mTEC II cells expressed the highest number of variable and uncorrelated genes (Fig. 3a, b and Extended Data Fig. 6). Notably, mTEC III cells showed a high level of stochastic gene expression (Fig. 3a–c) in spite of low expression of AIRE. MARS-seq analysis of 1,332  $CD45^- EpCAM^+$  single cells from *Aire* knockout mice, validated that AIRE deficiency almost entirely eliminated the expression of the ‘stochastic’ genes within the mTEC II and III populations (87% and 67%, respectively; Fig. 3e and Extended Data Fig. 6). In addition, AIRE deficiency also resulted in a decrease in mTEC I and mTEC III populations (Fig. 3f). By contrast, mTEC II cells and cTECs, showed an increase in frequency, while the mTEC IV population was unaffected (Fig. 3f). In order to better understand the lineage relationships of the individual mTEC subsets we performed *in vivo* fate mapping using *Csnb*<sup>cre</sup>*Rosa26*<sup>tdTomato</sup> reporter mice (Extended Data Fig. 6

and Methods). Whereas *Csnb* (also known as *Csn2*) expression was restricted to the mTEC II and III subsets (Fig. 3g and Extended Data Fig. 6), the *tdTomato* reporter was expressed in mTEC II, III and IV, but was absent from mTEC I cells (Fig. 3h and Extended Data Fig. 6). This suggests that while mTEC IV cells may be developmentally derived from the *Csnb*<sup>+</sup> mTEC II and/or III populations, or from a common ancestor, the mTEC I population is not.

Molecularly, the mTEC IV population is distinct from the other mTEC subsets, including the chromatin state, gene-expression profile and lack of stochastic gene expression (Figs. 1–3). On the basis of these data, we hypothesized that it may have a different functional role. This was further supported by specific expression of several genes that are associated with a rare epithelial lineage that is found in the gut, known as tuft (brush) cells<sup>14–16</sup> (Extended Data Fig. 7). In order to validate whether mTEC IV cells represent a putative tuft cell type, we compared their transcriptional profile to intestinal tuft cells and to the different TEC populations. Notably, mTEC IV cells were more similar to intestinal  $Hpgds-tdTomato^+$  tuft cells than to any of the TEC subpopulations (Fig. 4a). Specifically, mTEC IV cells and intestinal tuft cells shared a large number of regulatory factors and tuft cell-specific genes including *Avil*, *Il25* and *Pou2f3*. However, they also showed differential gene

expression, including for *Gp2* and *Gnb3*, which were only expressed in mTEC IV cells (Fig. 4b, c and Extended Data Fig. 7). Moreover, microscopy analysis of mTEC IV cells showed a typical tuft-like staining pattern in samples from both mice and humans (Fig. 4d, e). Finally, deficiency of a master regulator of intestinal tuft cells, *Pou2f3*, resulted in the complete loss of the mTEC IV population without affecting the development of any other TEC population (Fig. 4f, g and Extended Data Fig. 8), suggesting that they represent a bona fide tuft cell population.

Because the mTEC IV population is characterized by high and exclusive expression of IL-25 in the stroma of the thymus (Fig. 4b), we next studied their potential impact on thymic cells expressing the IL-25 receptor (*IL17rb*) (Fig. 4h). To this end, we first characterized 3,500 thymic CD45<sup>+</sup>IL-25R<sup>+</sup> cells using MARS-seq and found five different subpopulations with distinct transcriptional states, including several CD3<sup>+</sup> thymocyte subsets, as well as thymus-resident type-2 innate lymphoid cells (ILC2s) (Fig. 4h–j and Extended Data Fig. 9). Notably, the loss of mTEC IV cells in *Pou2f3*<sup>−/−</sup> mice was accompanied by a significant increase in the thymic ILC2 population (Fig. 4k), whereas it had no significant impact on other thymic CD45<sup>+</sup>IL-25R<sup>+</sup> cells or the main T cell subsets (Extended Data Fig. 9). The increase in the ILC2 (Lin<sup>−</sup>TCR<sup>−</sup>CD127<sup>high</sup>Tbet<sup>−</sup>RORγt<sup>−</sup>GATA3<sup>+</sup>) subset in *Pou2f3*<sup>−/−</sup> versus wild-type mice was further confirmed by conventional flow cytometry (Fig. 4l and Extended Data Fig. 9).

In summary, our study provides a comprehensive atlas of the stromal populations in the thymus of adult mice and during differentiation. We uncover unexpected complexity and diversity in this compartment, including an mTEC population with tuft-cell characteristics. This study also highlights important qualitative differences between the embryonic and postnatal thymus, which have, thus far, remained uncharacterized. As such, it clarifies many past controversies and confusions about the molecular, developmental and functional characteristics of the previously characterized TEC subsets and TRA expression, enabling the field to progress forward on a stable and common molecular blueprint. Nevertheless, several important open questions remain to be addressed in the future, including other functions of the mTEC IV population in the thymus and the lineage relationship and origins of the individual TEC subsets. Specifically, whether the mTEC II, III and IV populations are derived from a common ancestor cell, or whether mTEC IV cells are derived from the mTEC II and/or III populations.

## Online content

Any Methods, including any statements of data availability and Nature Research reporting summaries, along with any additional references and Source Data files, are available in the online version of the paper at <https://doi.org/10.1038/s41586-018-0346-1>.

Received: 5 September 2017; Accepted: 6 June 2018;

Published online: 18 July 2018

1. Klein, L., Kyewski, B., Allen, P. M. & Hogquist, K. A. Positive and negative selection of the T cell repertoire: what thymocytes see (and don't see). *Nat. Rev. Immunol.* **14**, 377–391 (2014).
2. Abramson, J. & Anderson, G. Thymic epithelial cells. *Annu. Rev. Immunol.* **35**, 85–118 (2017).
3. Takahama, Y., Ohigashi, I., Baik, S. & Anderson, G. Generation of diversity in thymic epithelial cells. *Nat. Rev. Immunol.* **17**, 295–305 (2017).
4. Jaitin, D. A. et al. Massively parallel single-cell RNA-seq for marker-free decomposition of tissues into cell types. *Science* **343**, 776–779 (2014).
5. Paul, F. et al. Transcriptional heterogeneity and lineage commitment in myeloid progenitors. *Cell* **163**, 1663–1677 (2015).

6. Takada, K. & Takahama, Y. Positive-selection-inducing self-peptides displayed by cortical thymic epithelial cells. *Adv. Immunol.* **125**, 87–110 (2015).
7. Wong, K. et al. Multilineage potential and self-renewal define an epithelial progenitor cell population in the adult thymus. *Cell Rep.* **8**, 1198–1209 (2014).
8. Galliano, M. F. et al. Characterization and expression analysis of the *Spink5* gene, the mouse ortholog of the defective gene in Netherton syndrome. *Genomics* **85**, 483–492 (2005).
9. Hale, L. P. & Markert, M. L. Corticosteroids regulate epithelial cell differentiation and Hassall body formation in the human thymus. *J. Immunol.* **172**, 617–624 (2004).
10. Lara-Astiaso, D. et al. Chromatin state dynamics during blood formation. *Science* **345**, 943–949 (2014).
11. Buenrostro, J. D., Giresi, P. G., Zaba, L. C., Chang, H. Y. & Greenleaf, W. J. Transposition of native chromatin for fast and sensitive epigenomic profiling of open chromatin, DNA-binding proteins and nucleosome position. *Nat. Methods* **10**, 1213–1218 (2013).
12. Brennecke, P. et al. Single-cell transcriptome analysis reveals coordinated ectopic gene-expression patterns in medullary thymic epithelial cells. *Nat. Immunol.* **16**, 933–941 (2015).
13. Meredith, M., Zemmour, D., Mathis, D. & Benoist, C. Aire controls gene expression in the thymic epithelium with ordered stochasticity. *Nat. Immunol.* **16**, 942–949 (2015).
14. Gerbe, F. et al. Distinct ATOH1 and Neurog3 requirements define tuft cells as a new secretory cell type in the intestinal epithelium. *J. Cell Biol.* **192**, 767–780 (2011).
15. Gerbe, F. et al. Intestinal epithelial tuft cells initiate type 2 mucosal immunity to helminth parasites. *Nature* **529**, 226–230 (2016).
16. Gerbe, F., Brulin, B., Makrini, L., Legraverend, C. & Jay, P. DCAMKL-1 expression identifies tuft cells rather than stem cells in the adult mouse intestinal epithelium. *Gastroenterology* **137**, 2179–2180 (2009).

**Acknowledgements** I.A. is supported by the Chan Zuckerberg Initiative, the HHMI International Scholar award, the European Research Council Consolidator Grant (ERC-COG)724471-HemTree2.0, the Israel Science Foundation (703/15), the Ernest and Bonnie Beutler Research Program of Excellence in Genomic Medicine, the Helen and Martin Kimmel award for innovative investigation, a Minerva Stiftung research grant, the Israeli Ministry of Science, Technology, and Space, the David and Fela Shapell Family Foundation, the NeuroMac DFG/Transregional Collaborative Research Center Grant, and the Abramson Family Center for Young Scientists. I.A. is the incumbent of the Alan and Laraine Fischer Career Development Chair. J.A. is supported by the ERC-2016-CoG-724821, Israel Science Foundation (1796/16 and 722/14), the Sy Syms Foundation; US-Israel Binational Foundation, Maurice and Vivienne Wohl Charitable Foundation; Goodman Family Charitable Lead Annuity Trust; Ruth and Samuel David Gameroff Family Foundation. J.A. is an incumbent of the Dr. Celia Zwillenberg-Fridman and Dr. Lutz Fridman Career Development Chair; A.G. is a recipient of the Clore fellowship; N.T., P.J. and V.Z. are supported by ANR-17-CE15-TUFTEFF, the Labex EpiGenMed and SIRIC Montpellier Cancer Grant INCa\_Inserm\_DGOS\_12553; M.P. is supported by the Labex EpiGenMed and the FRM; F.G. and V.Z. are supported by CNRS; and N.T. and P.J. are supported by Inserm. We thank M. Boyer-Clavel and S. Gailhac of Montpellier Rio Imaging for cell sorting and the RAM animal facility of the IGMM.

**Author contributions** C.B., S.N., A.G., N.K., J.A. and I.A. designed the project, planned the experiments and wrote the manuscript. C.B., S.N. and N.K. performed experiments, A.G. and E.D. analysed the data, M.P., F.G., A.M., N.T., P.J. and V.Z. performed intestinal tuft and *Pou2f3* knockout mouse experiments. A.C. generated the *Csnb*-reporter mouse. B.T. and S.I. contributed to the single-molecule RNA fluorescence in situ hybridization experiment. O.G. provided human samples.

**Competing interests** The authors declare no competing interests.

## Additional information

**Extended data** is available for this paper at <https://doi.org/10.1038/s41586-018-0346-1>.

**Supplementary information** is available for this paper at <https://doi.org/10.1038/s41586-018-0346-1>.

**Reprints and permissions information** is available at <http://www.nature.com/reprints>.

**Correspondence and requests for materials** should be addressed to J.A. or I.A. **Publisher's note:** Springer Nature remains neutral with regard to jurisdictional claims in published maps and institutional affiliations.

## METHODS

**Data reporting.** No statistical methods were used to predetermine sample size. The experiments were not randomized and the investigators were not blinded to allocation during experiments and outcome assessment.

**Mice.** All mice were maintained under specific pathogen-free conditions at the Weizmann Institute's animal facility and were handled in accordance with the guidelines of the Institutional Animal Care and Use Committee (25720316-2). Wild-type C57BL/6 (B6) mice were purchased from Harlan Laboratories. *Aire* knockout C57BL/6 mice were purchased from Jackson Laboratories. *Sox9<sup>GFP</sup>* mice were generated as described previously<sup>17</sup>. *Pou2f3* knockout and *Hpgds<sup>tdTomato</sup>* mice were maintained under pathogen-free conditions at the IGMM and IGF animal facilities (RAM). *Csnb<sup>cre</sup>* mice were generated using bacterial artificial chromosome (BAC) recombination. In brief, homology arms corresponding to a sequence downstream to the ATG of the *Csnb* gene were cloned into a Cre-recombinase-coding plasmid (pConst-Cre; provided by G. Schutz), followed by homologous recombination of the *cre* coding sequence into the BAC containing the *Csnb* gene (RP23-218H23, CHORI). Flp recombination was then used to remove the antibiotic resistance cassette. The final BAC was injected into fertilized BALB/c oocytes by the Weizmann transgenic core facility. Heterozygous mutants were backcrossed to C57BL/6 mice. *Csnb<sup>cre</sup>Rosa26<sup>tdTomato</sup>* reporter mice were generated by breeding heterozygous *Csnb<sup>cre</sup>* mice with *Rosa26<sup>tdTomato</sup>* mice (Jackson Laboratories).

**Human samples.** Human thymus samples were obtained during the course of corrective cardiac surgery at Schneider Children's Medical Center of Israel, following ethical approval (0781-16-RMC). An informed consent was signed by parents of the patients before obtaining the thymus.

**Ethical compliance.** All animals were housed according to guidelines at the Weizmann Institute of Science and the IGMM and IGF animal facilities (RAM). All experimental procedures were approved by the Institutional Animal Care and Use Committee (IACUC), application number 25720316-2.

All human experiments were done according to guidelines at the Weizmann Institute of Science and approved by Helsinki ethics committee, approval number 0781-16-RMC.

**Isolation of mouse thymic stromal cells.** Thymi from 4–8-week-old mice (unless otherwise stated, for embryonic or neonatal thymi) were placed into cold 1 × PBS supplemented with 2% fetal bovine serum (FBS, Invitrogen). Thymi were chopped into small pieces and disintegrated by enzymatic digestion for 30–40 min in a 37°C water bath, using 0.3 mg ml<sup>-1</sup> collagenase D (Roche, 1088858), 1 mg ml<sup>-1</sup> dispase II (Roche, 04942078001) and 10 ng ml<sup>-1</sup> DNase I (Sigma-Aldrich, DN25) in RPMI supplemented with 2% FBS. Cells were then filtered through a 50-µm mesh filter and washed with 5–10 ml MACS buffer (1 × PBS with 5 mM EDTA and 2% FBS), followed by centrifugation at 230g for 4 min. Percoll gradient density centrifugation was performed in order to enrich the stromal compartment. In brief, cells were resuspended in 2 ml of 1.115 g ml<sup>-1</sup> isotonic Percoll (Sigma-Aldrich, P1644) and placed at the bottom of a tube. Subsequently, 1 ml of isotonic 1.065 g ml<sup>-1</sup> Percoll and then 1 ml of 1 × PBS were layered on top. The Percoll gradient was centrifuged at 2,700 r.p.m., 4°C, with no deceleration for 30 min. The thymic stroma accumulated between the top and middle layers, and was collected and washed with MACS buffer and centrifuged at 230g for 4 min. Embryonic thymi were not subjected to Percoll separation, but were treated with red blood cell lysis buffer (15 mM ammonium chloride, 1 mM potassium bicarbonate, 10 µM EDTA in double distilled water, pH 7.3).

**Isolation of thymic haematopoietic cells.** Thymi from 6–12-week-old mice were surgically removed and placed in PBS on ice. Thymi were trimmed of fat and connective tissues, and thymocytes were extracted into a single-cell suspension by pressing the thymic lobes against a 70-µm cell strainer. Cells were washed in MACS buffer (1 × PBS with 2% FBS and 5 mM EDTA pH 8.0).

**Isolation of intestinal epithelial cells.** Mouse small intestines were isolated, flushed with PBS and incised along their length. The tissue was incubated in 30 mM EDTA (Sigma-Aldrich) in HBSS pH 7.4 (Life Technologies) on ice, and transferred to DMEM (Life Technologies) supplemented with 10% FBS (Sigma-Aldrich). Vigorous shaking yielded the epithelial fraction that was then incubated with 100 µl of dispase (BD Biosciences) in 10 ml of HBSS, supplemented with 100 µl of DNase I at 2,000 Kunitz (Sigma). The single-cell preparation was obtained by filtration through a 30-µm mesh and used for further staining.

**Antibodies and reagents for flow cytometry.** APC–Cy7–EPCAM (118218), PE–Ly51 (108308), Pacific blue–I-A/I-E (107620), PerCP–Cy5.5–CD45 (103132), FITC–CD34 (343603), APC–CD31 (102409), PE–Cy7–CD45 (103114), FITC–ITGB4 (123605), PE–ITGB4 (123610) and PE–IL-17RB (IL-25R, 146305) were purchased from Biolegend; APC–L1CAM (FAB5674R) was purchased from Novus; APC–GATA3 (560078), brilliant violet 650–ROR-γt (564722), biotinylated CD3 (553060), biotinylated CD4 (553728), biotinylated CD8 (553029), biotinylated B220 (553086), biotinylated Ter119 (553672), biotinylated CD11c (553800), biotinylated Gr1 (553125), FITC–CD45 (553080), FITC–CD8 (553031), APC–Ter119 (557909), PE–Cy7–CD45 (552848), brilliant violet 711–CD4 (563726),

APC–CD8 (553035), horizon V500–CD44 (560780), brilliant violet 711–Tcrγ (563994) and horizon V450–Tcrβ (560706) were purchased from BD; and PerCP–eFluor710–Ly6d (46-5974-80), PE–Cy7–CD127 (25-1273-82), PE–Tbet (12-5825-82), eFluor780–CD4 (47-0042-82) and eFluor780–CD25 (47-025182) were purchased from eBioscience. The following materials were also used for FACS staining: 7-AAD Viability Staining Solution (Biolegend, 420404); Biotinylated Ulex Europaeus Agglutinin I (UEA I) (Vector laboratories, B-1065), PE–Cy7–streptavidin (405206, Biolegend), PerCP–Cy5.5–streptavidin (554064, BD), SYTOX (S34857, Invitrogen), FcR blocker (BE0307, Bio X Cell).

**Flow cytometry and sorting.** Cells were stained in MACS buffer (1 × PBS with 2% FBS and 5 mM EDTA pH 8.0) with specific antibodies for 30 min at 4°C. For haematopoietic cells, to avoid non-specific binding of antibodies to Fcγ receptors, anti-mouse CD16/CD32 monoclonal antibody (Bio X cell, BE0307 or Biolegend, 10130) was added to the antibody mix. Following staining, cells were washed and resuspended in MACS buffer. Secondary staining with streptavidin was performed in a similar manner. After the wash, cells intended for intracellular staining were fixed and permeabilized using the eBioscience fixation/permeabilization kit according to kit instructions, and stained with antibodies of intracellular markers for 2 h at 4°C. Cells were sorted on a BD FACSARIA Special Order Research Product (SORP) or BD FACSARIA Fusion/II or III, or analysed on a BD LSRFortessa or BD FACSCantoII. Spectral overlap between fluorescent dyes was compensated using single-stained controls. Pre-gating was first done for live cells (in non-fixed samples) based on a 7-AAD, DAPI or SYTOX stain, followed by single-cell gating according to the FSC-A versus FCS-W plot. Data analysis was performed using FlowJo software (Tree Star Inc.).

mTEC subsets (Fig. 2a) were sorted from CD45<sup>+</sup>EPCAM<sup>+</sup> cells using the following sub-sorting gates: mTEC I: MHC-II<sup>low</sup>ITGB4<sup>+</sup>L1CAM<sup>+</sup>; mTEC II: MHC-II<sup>+</sup>Ly6d<sup>+</sup>; mTEC III: ITGB4<sup>+</sup>L1CAM<sup>+</sup>Ly6d<sup>+</sup>; mTEC IV: MHC-II<sup>low</sup>L1CAM<sup>+</sup>.

**Single-cell index sorting.** Isolated cells were single-cell sorted into 384-well cell capture plates containing 2 µl of lysis solution and barcoded poly(T) reverse-transcription primers for single-cell RNA-seq. Barcoded single-cell capture plates were prepared with a Bravo automated liquid handling platform (Agilent), as described previously<sup>4</sup>. To record marker levels of each single cell, the FACS Diva 7 'index sorting' function was activated during single-cell sorting.

**Library preparation for single-cell RNA sequencing.** Single-cell libraries were prepared as previously described<sup>4</sup>. In brief, 384-well plates, which contained lysis buffer and barcoded reverse-transcription poly-T primers, were immediately spun down and placed on dry ice. For barcoding and reverse transcription, a reverse-transcription reaction mix was added and the plates were placed in a PCR machine set to the appropriate program. All barcoded samples were pooled, followed by addition of exonuclease to remove excess RT-PCR primers. A purification step using SPRI beads that bind cDNA and RNA was performed after this step, as well as after each of the following steps. The pooled single-stranded cDNA was converted to a double-stranded DNA using a designated kit, in order to perform in vitro transcription of RNA molecules. The template DNA was then removed using DNase, and the generated RNA was fragmented and ligated to barcoded Illumina adapters. Reverse transcription of this ligation product was done using primers specific for the Illumina adapters, and libraries of the resulting cDNA were generated and enriched by 12–15 PCR cycles.

**Low-level processing and filtering.** All RNA-seq libraries (pooled at equimolar concentration) were sequenced using the Illumina NextSeq 500 at a median sequencing depth of 16,289 reads per single cell. Sequences were mapped to mouse genome (mm9), demultiplexed and filtered as previously described<sup>4,18</sup>, extracting a set of unique molecular identifiers (UMI) that define distinct transcripts in single cells for further processing. We estimated the level of spurious UMIs in the data using statistics on empty MARS-seq wells (median noise 2.8%; Extended Data Fig. 2). Mapping of reads was done using HISAT (version 0.1.6)<sup>19</sup>; reads with multiple mapping positions were excluded. Reads were associated with genes if they were mapped to an exon, using the UCSC genome browser as reference. Exons of different genes that shared genomic position on the same strand were considered a single gene with a concatenated gene symbol. Cells with less than 500 UMIs were discarded from the analysis. After filtering, cells contained a median of 1,711 unique molecules per cell.

**Data processing and clustering.** The MetaCell pipeline was used to derive informative genes and compute cell-to-cell similarity, to compute KNN graph covers and derive distribution of RNA in cohesive groups of cells (or metacells), and to derive strongly separated clusters using bootstrap analysis and computation of graph covers on resampled data. The MetaCell package is described in detail in Supplementary Note 1. Default parameters were used unless otherwise stated.

Clustering for Figs. 1, 2 was done on a combined set of cells from two sources: (1) 1,972 CD45<sup>+</sup> thymic cells and (2) 1,542 CD45<sup>+</sup>EPCAM<sup>+</sup> thymic cells (Extended Data Fig. 2). Clustering resulted in 49 clusters. Clusters with increased expression of *Hbb-b1*, *Trbc2* or *C1qb*, which are markers for red blood cells, T cells or macrophages, respectively (mean expression >10 times the median across clus-



ters), were marked as contaminants and discarded from further analysis (Extended Data Fig. 3). We performed hierarchical clustering over the clusters structure and divided clusters into epithelial, endothelial and fibroblast groups by cutree.

**Mapping cells to an existing cluster model.** Given an existing reference single-cell dataset and cluster model, and a new set of single-cell profiles, we extracted for each new cell the  $K$  ( $K = 10$ ) reference cells with top Pearson correlation on transformed marker gene UMIs as described above. The distribution of cluster memberships over these  $K$ -neighbours was used to define the new cell reference cluster (by majority voting), and was applied for visualizing new cells by weighted average of the  $x$  and  $y$  coordinates of the clusters.

**Clustering of development TEC and comparison to the existing model.** Clustering of TEC during embryonic and postnatal development (Fig. 3) was done on a combined dataset of 1,343 E14.5, 895 E18.5 and 836 6 days postnatal epithelial cells. Two-dimensional projection of the resulting clustering was produced by MetaCell. However, in order to maintain the structure of the two-dimensional projection in Fig. 2, while enabling the discovery of new transcriptional states, we computed the KNN structure of the combined developmental and mature TEC. Developmental clusters with more than 20% cells for which >20% of their neighbours are within the mature dataset were associated with the mature projection, and their two-dimensional coordinates were determined by their mature neighbours. All other developmental clusters were assigned their regular coordinates (Fig. 3a and Extended Data Fig. 6).

For further refinement of the early TEC population (as in Fig. 3g), all developmental metacells with mean expression >0.25 times the median across clusters were included.

**Gene modules and cell cycle analysis.** Identification of ribosomal, cell cycle or other broadly expressed gene modules was done by clustering genes in a downsampled UMI matrix (500 molecules per cell). We filtered genes with total molecule (UMI) count lower than 5 and variance-to-mean ratio lower than 1.2. Hierarchical clustering using Ward's method was performed for detecting 30 fine-grained clusters. After removing clusters with mean Pearson intracorrelation lower than 0.025, 26 gene modules were retained. Manual annotation of the gene clusters was performed. This resulted in the identification of 26 modules with 8–136 genes, among which the cell cycle module contained 73 genes. Ribosomal modules (86 genes) were excluded from clustering analysis. Expression of cell cycle genes is a good indicator of proliferation<sup>20</sup>. To determine proliferation status of genes, we examined the pooled normalized expression of the cell cycle module across genes. This measurement showed a bimodal distribution, correlating with the total UMI count of cells (Extended Data Fig. 4e).

**GO enrichment.** Gene enrichment analysis was done using metaspice software with mouse whole-genome backup.

**Analysis of stochastically expressed genes.** In order to define stochastically expressed genes, genes with less than 50 total UMIs were discarded (list A). Of this list, genes for which the corrected variance was greater than 1 (by a linear fit of the variance to the mean expression) were defined as variably expressed (list B). Gene-to-gene Pearson correlations were then computed on the UMI values of genes from list B (normalized to cell size). In order to discard tightly correlated gene expression programs, only genes for which the third highest correlation with other genes was less than 0.25 were considered as stochastically expressed (list C; Supplementary Table 4).

An established list of TRA genes was taken from a previous publication<sup>21</sup>. AIRE dependency of these TRA was determined by a twofold reduction in *Aire* knockout mice measured in the previous study<sup>21</sup>. Both AIRE-dependent and -independent lists were intersected with list B for further analysis.

**Immunofluorescence staining of frozen thymic sections.** Thymi from 4–8-week-old female mice were embedded in OCT compound (Tissue-Tek, Sakura) and frozen on dry ice. Cryostat sections (6  $\mu$ m) were fixed with ice-cold acetone for 10 min and incubated with primary antibody (anti-AIRE AF488-conjugated, 04-150; Millipore) diluted in 1% BSA in PBS for 60 min at room temperature. Sections were washed three times with PBS and incubated with DAPI staining for 10 min at room temperature, followed by three washes with PBS.

**Immunofluorescence staining of PFA-fixed frozen thymic sections.** Thymi from 4–8-week-old wild-type, *Sox9<sup>GFP</sup>*, *Csnb<sup>cre</sup>+Rosa26<sup>tdTomato</sup>* and *Csnb<sup>cre</sup>-Rosa26<sup>tdTomato</sup>* mice were isolated, cleaned and fixed for 3 h with ice-cold 3.7% formaldehyde, followed by overnight incubation with cryoprotection solution (3.7% formaldehyde, 30% sucrose in 1 $\times$  PBS). Thymi were embedded in OCT and frozen on dry ice. Cryostat sections (6–7  $\mu$ m) were permeabilized and blocked with blocking buffer (TBS, pH 7.4, 5% goat serum or BSA, and 0.1% Triton X-100) for 30 min at room temperature. Sections were then incubated with primary antibodies diluted in blocking buffer overnight at 4°C. Primary antibodies used were as follows: anti-PSMB11 (pd021, MBL); anti-PIGR (AF2800, R&D Systems); anti-DCLK1 (ab37994, Abcam); APC-conjugated anti-ITGA6 (313615; Biolegend). Sections were washed twice with TBST (1 $\times$  TBS supplemented with 0.1% Tween-20). Sections stained with unconjugated antibodies were incubated with a second-

ary antibody (goat anti-rabbit AF555, Jackson Laboratories) for 60 min at room temperature. DAPI staining was performed for 10 min at room temperature.

**Immunofluorescence staining of paraffin-embedded thymic sections.** Thymi from 4–8-week-old mice or 8-day-old male humans were fixed in 4% PFA for 48 h, followed by embedding in paraffin. Subsequently, 5- $\mu$ m-thick sections were dewaxed in xylene and rehydrated in graded alcohol baths. Antigen retrieval was performed by boiling slides for 20 min in 10 mM sodium citrate buffer, pH 6.0. Nonspecific binding sites were blocked in blocking buffer (TBS pH 7.4, 5% goat serum and 0.1% Triton X-100) for 30 min at room temperature. Sections were incubated with primary antibodies diluted in blocking buffer overnight at 4°C. Primary antibodies used were as follows: anti-VILLIN (MAB1671, Millipore); anti-COX1 (sc-1754, Santa Cruz Biotechnology); anti-DCLK1 (ab37994, Abcam). Slides were washed two times with TBST before incubation with fluorescent secondary antibodies conjugated to AF488, AF555, Cy3 or Cy5 (Jackson ImmunoResearch Laboratories) and Hoechst (Sigma-Aldrich) or DAPI in TBS–0.1% Triton X-100.

**Single-molecule RNA fluorescence in situ hybridization (FISH).** Single-molecule FISH probe libraries consisting of 48 probes with a length of 20 bp were designed as previously described<sup>22</sup>, constructed and provided by Agentek. The following probe libraries were used: *Avil*, *Sbsn* coupled to Cy5, *Epcam* and *Pigr* coupled to AF594. RNA FISH was performed as previously described. In brief, thymi from 4–8-week-old female mice were isolated, cleaned and fixed for 3 h with ice-cold 3.7% formaldehyde followed by overnight incubation with cryoprotection solution (3.7% formaldehyde, 30% sucrose in PBS). Thymi were embedded in OCT and frozen on dry ice. Cryostat sections (5–8  $\mu$ m) were air-dried and fixed again with 3.7% formaldehyde for 5 min following by 2 h incubation with 70% ethanol at 4°C. Sections were rehydrated with 2 $\times$  SSC, and treated with proteinase K in 2 $\times$  SSC for 10 min at room temperature. Hybridization was performed overnight by 20% formamide in 2 $\times$  SSC with 0.1 ng  $\mu$ l<sup>-1</sup> of the desired probes at 30°C. DAPI (to stain the nuclei) was added during the washes, and sections were incubated with fresh GLOX buffer (10 mM Tris pH 8.0 and 0.4% glucose in 2 $\times$  SSC).

**Imaging and image analysis.** Imaging was performed on Ultima Multiphoton Microscope, Nikon Eclipse TI-S fluorescence microscope, or Nikon-Ti-E inverted fluorescence microscope with 60 $\times$  and 100 $\times$  oil-immersion objectives and a Photometrics Pixis 1024 CCD camera, using MetaMorph software (Molecular Devices) or NIS element software (Nikon). Image analysis was performed with ImageJ software.

**Indexing first chromatin immunoprecipitation followed by deep sequencing (iChIP-seq).** iChIP-seq was prepared as previously described<sup>10</sup>. In brief, cells were cross-linked for 8 min in 1% formaldehyde and quenched for 5 min in 0.125 M glycine before sorting. Cells were sorted using the described sorting strategy and frozen. Cell pellets were lysed in 0.5% SDS and sheared with the NGS Bioruptor Sonicator (Diagenode). Sheared chromatin was immobilized on 15  $\mu$ l Dynabeads Protein G (Invitrogen) with 1.3  $\mu$ g of anti-H3 antibody (Abcam). Magnetized chromatin was then washed with 10 mM Tris-HCl supplemented with 1 $\times$  PI. Chromatin was end-repaired, dA-tailed and ligated with sequencing adapters containing Illumina P5 and P7 sequences. Indexed chromatin was pooled and incubated with 2.5  $\mu$ g H3K4me2 antibody (ab32356, Abcam) at 4°C for 3 h and for an additional hour with protein G magnetic beads (Invitrogen). Magnetized chromatin was washed and reverse cross-linked. DNA was subsequently purified with 1.65 $\times$  SPRI and amplified by PCR with 0.5  $\mu$ M of forward and reverse primers containing Illumina P5-rd1 and P7-rd2 sequences. Library concentration was measured with a Qubit fluorometer and mean molecule size was determined by TapeStation (Agilent). DNA libraries were sequenced on an Illumina NextSeq 500 with an average of over 10 million aligned reads per replicate.

**ATAC-seq.** To profile open chromatin, we used an assay of transposase-accessible chromatin following sequencing (ATAC-seq) as previously published<sup>23</sup>, with modifications as previously described<sup>10</sup>. In brief, cell populations were sorted in 400  $\mu$ l of MACS buffer (1 $\times$  PBS, 0.5% BSA, 2 mM EDTA) and pelleted by centrifugation for 15 min at 500g and 4°C with low acceleration and brake settings. Cell pellets were washed once with 1 $\times$  PBS and cells were pelleted by centrifugation using the previous settings. Cell pellets were resuspended in 25  $\mu$ l of lysis buffer (10 mM Tris-HCl (pH 7.4), 10 mM NaCl, 3 mM MgCl<sub>2</sub>, 0.1% Igepal CA-630) and nuclei were pelleted by centrifugation for 30 min at 500g, 4°C with low acceleration and brake settings. Supernatant was discarded and nuclei were resuspended in 25  $\mu$ l reaction buffer containing 2  $\mu$ l of Tn5 transposase and 12.5  $\mu$ l of TD buffer (Nextera Sample preparation kit from Illumina). The reaction was incubated at 37°C for 1 h. Then, 5  $\mu$ l of clean-up buffer (900 mM NaCl, 300 mM EDTA), 2  $\mu$ l of 5% SDS and 2  $\mu$ l of Proteinase K (NEB) were added and incubated for 30 min at 4°C. Tagmented DNA was isolated using 2 $\times$  SPRI beads clean-up. For library amplification, two sequential nine-cycle PCR runs were performed in order to enrich small tagmented DNA fragments. We used 2  $\mu$ l of indexing primers included in the Nextera Index kit and KAPA HiFi HotStart ready mix. After the first PCR, the libraries were selected for small fragments (less than 600 bp) using SPRI clean-up. Then a second PCR was performed with the same conditions in order to obtain the final library.

**Processing of iChIP-seq, ATAC-seq and chromatin peak calling.** Reads were aligned to the mouse reference genome (mm9, NCBI v.37) using Bowtie aligner version 1.0.0<sup>24</sup> with best match parameters (bowtie -m 1 -sam -best -strata -v 2). To identify regions of enrichment (peaks) from ChIP-seq reads of H3K4me2, we used the HOMER package makeTagDirectory followed by the findPeaks command with the histone parameter<sup>25</sup> and IDR filtering for reproducible peaks across replicates<sup>26</sup>. Union peaks file were generated by combining and merging overlapping peaks in all samples.

**Chromatin analysis.** For clustering of differential peaks, we first averaged peak sizes across replicates. We defined differential peaks as peaks for which the maximum value is more than fourfold higher than their minimum value. We then normalized peaks intensities and performed K means clustering ( $K = 7$ ). For motif finding, we independently called peaks in ATAC-seq, as above, and identified the maximum peak that overlapped each H3K4me2 region. The overlapping sequences were input for HOMER package motif finder algorithm findMotifGenome<sup>25</sup>.

**Gene tracks and visualization.** All gene tracks were visualized as bigWig files of the combined replicates normalized to 10,000,000 reads, using Integrative Genomics Viewer (<http://www.broadinstitute.org/igv>).

**Real-time PCR analysis.** Cells were sorted into 40–50  $\mu$ l of lysis/binding buffer (Life Technologies). mRNA was captured with 15  $\mu$ l of Dynabeads oligo(dT) (Life Technologies), washed and eluted at 85 °C with 10  $\mu$ l of 10 mM Tris-Cl (pH 7.5). The purified RNA was used for cDNA synthesis using the High-Capacity cDNA Reverse-Transcription kit (Applied Biosystems) and polyT primers. The subsequent qPCR analysis was performed using the Fast SYBR Green Master Mix (Life technologies). Differential expression was calculated according to the  $\Delta\Delta C_t$  method. Specific qPCR primers: *Actb*: GGAGGGGGTTGAGGTGTT, TGTGCACTTTTATTGGTCTCAAG; *Sox4*: GCTGGGCTTTCTCCTCCT, AGGCTGGCCTGCTACTCC; *Aire*: TGGGCTGATTAGGACCAAGA, ACAAAGATCAGGGCCATCTG; *Avil*: GCATCAGGACCCACATCTGC, ATGCTGTGGCACATGGTAGAC; *Sbsn*: CACCATGCCCTAAACTGATGC, ACAAAGCTCAAAGCAGCCCTC; *cre*: AGGAGAATGTGGATGCTGGGG, CAATTTTCGGCAATGCGCAGC; *Csnb*: AAACCTCAGAAGGTGAATCTCATGG, GCTGGATGTTTTGTGGGACG.

**Lists of ribosomal and cell cycle modules.** *Ribosomal genes.* 2810422J05Rik, AC151602.1, AL663027.1, Cfl1, Eef1b2, Ftl1, Gm10059, Gm10076, Gm10443, Gm11361, Gm11808, Gm11942, Gm12630, Gm13408, Gm14456, Gm15427, Gm15459, Gm15710, Gm3788, Gm4149, Gm5244, Gm5559, Gm8730, Gm8759, Gnb2l1, Hspa8, Mif, Rpl10, Rpl13, Rpl13a, Rpl14, Rpl18a, Rpl22, Rpl26, Rpl28-ps3, Rpl29, Rpl32, Rpl34, Rpl37, Rpl37a, Rpl38, Rpl38-ps2, Rpl4, Rpl7a-ps12, Rpl8, Rpl9-ps6, Rplp0, Rplp1, Rplp2, Rps10, Rps10-ps1, Rps14, Rps15, Rps18, Rps19, Rps2, Rps20, Rps21, Rps26, Rps28, Rps3, Rps3a, Rps5, Rps8, Rps9, Rpsa, Rpsa-ps10, Snord35a, Tmsb10, Tpt1, B2m, Eef1a1, Gas5, Gm13456, Gm15500, Gm16247, Rpl23, Rpl35a, Rpl7, Rps11, Rps24, Rps25, S100a11, Tmsb4x, Ubl5, mmu-mir-703.

*Cell cycle genes.* 2810417H13Rik, 2900006K08Rik, 4833427G06Rik, 4930473A06Rik, 5133401N09Rik, 6820408C15Rik, Arhgap11a, Arl6ip1, Birc5, Ccdc108, Ccdc113, Ccdc151, Ccdc17, Ccdc19, Ccdc30, Ccdc39, Ccdc40, Ccdc67, Ccno, Cdc20, Cdca8, Cenpf, Ckap2, Ckap2l, Cks1b, Dcdc2a, Dek, Dnahc9, Dnajb13, E030019B06Rik, Foxm1, Gm11423, Gm9938, H2afx, Hist1h1a, Hist1h1b, Hist1h1d, Hist1h1e, Hist1h2ac, Hist1h2ae, Hist1h2ao, Hist1h2ap, Hist1h3c, Hist1h3e, Hist1h4d, Hmgb2, Hnrnpa2b1, Ifi46, Kif15, Kif24, Lrrc23, Lrrc46, Mki67, Phospho2, Pih1d2, Plk1, Rsp1, Rsp19, Smc4, Supt16h, Tekt1, Tekt4, Tmem107, Top2a, Tll6, Tuba1b, Tubb2c, Tubb5, Ube2c, Wdr52, Wdr65, Zmynd10.

**Reporting summary.** Further information on experimental design is available in the Nature Research Reporting Summary linked to this paper.

**Code availability.** No custom software was used to collect data. iChIP-seq and ATAC-seq data analyses, including motif finding, were done with the HOMER package<sup>25</sup>. Single-cell data were analysed with the MetaCell package, which is available upon request.

**Data availability.** RNA, iChIP-seq and ATAC-seq data reported in this paper were deposited with Gene Expression Omnibus under accession numbers: GSE103967, GSE103968, GSE103969 and GSE103970.

- Tanimizu, N., Nishikawa, Y., Ichinohe, N., Akiyama, H. & Mitaka, T. Sry HMG box protein 9-positive (Sox9<sup>+</sup>) epithelial cell adhesion molecule-negative (EpCAM<sup>-</sup>) biphenotypic cells derived from hepatocytes are involved in mouse liver regeneration. *J. Biol. Chem.* **289**, 7589–7598 (2014).
- Gury-BenAri, M. et al. The spectrum and regulatory landscape of intestinal innate lymphoid cells are shaped by the microbiome. *Cell* **166**, 1231–1246 (2016).
- Kim, D., Langmead, B. & Salzberg, S. L. HISAT: a fast spliced aligner with low memory requirements. *Nat. Methods* **12**, 357–360 (2015).
- Scialdone, A. et al. Computational assignment of cell-cycle stage from single-cell transcriptome data. *Methods* **85**, 54–61 (2015).
- Sansom, S. N. et al. Population and single-cell genomics reveal the *Aire* dependency, relief from Polycomb silencing, and distribution of self-antigen expression in thymic epithelia. *Genome Res.* **24**, 1918–1931 (2014).
- Lyubimova, A. et al. Single-molecule mRNA detection and counting in mammalian tissue. *Nat. Protoc.* **8**, 1743–1758 (2013).
- Buenrostro, J. D., Wu, B., Chang, H. Y. & Greenleaf, W. J. ATAC-seq: a method for assaying chromatin accessibility genome-wide. *Curr. Protoc. Mol. Biol.* **109**, 21.29.1–21.29.9 (2015).
- Langmead, B., Trapnell, C., Pop, M. & Salzberg, S. L. Ultrafast and memory-efficient alignment of short DNA sequences to the human genome. *Genome Biol.* **10**, R25 (2009).
- Heinz, S. et al. Simple combinations of lineage-determining transcription factors prime cis-regulatory elements required for macrophage and B cell identities. *Mol. Cell* **38**, 576–589 (2010).
- Li, Q., Brown, J. B., Huang, H. & Bickel, P. J. Measuring reproducibility of high-throughput experiments. *Ann. Appl. Stat.* **5**, 1752–1779 (2011).

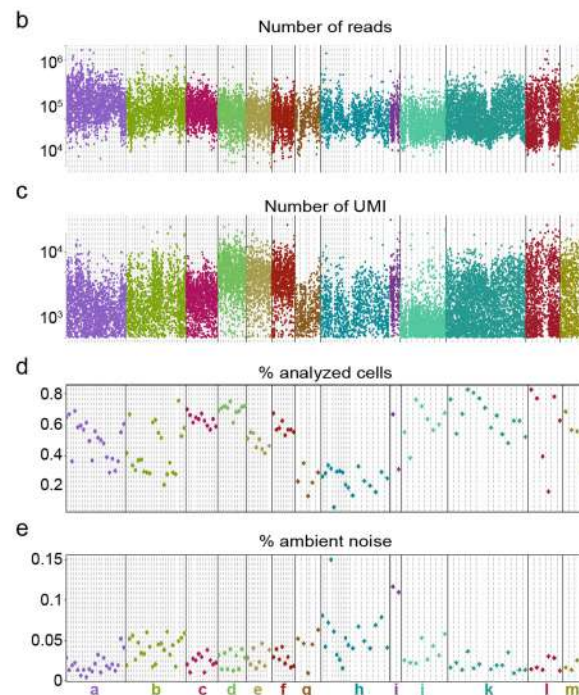


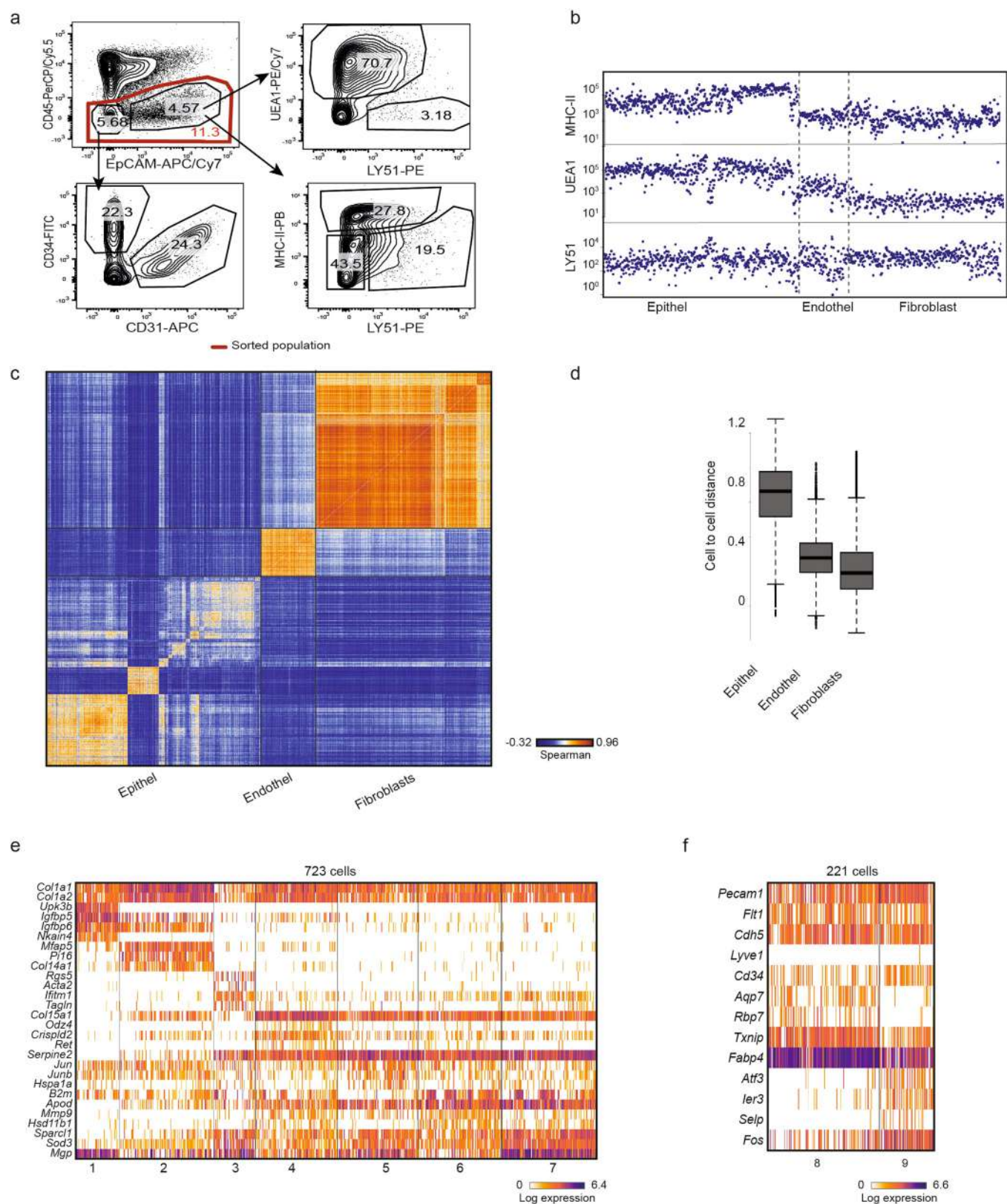
a

Organ	Gating	Age	Strain		Mouse	nbatches	ncells			
Thymus	CD45 <sup>+</sup>	4-6 weeks	WT	a	1	3	322			
					2	3	358			
					3	4	393			
					4	2	206			
					5	2	188			
					6	5	332			
					7	2	222			
	CD45 <sup>+</sup> EpCAM <sup>+</sup>	4-6 weeks	WT	b	8	2	208			
					9	4	267			
					10	3	168			
					11	4	443			
					12	2	95			
					13	3	178			
					14	2	246			
					15	1	111			
			Aire KO	c	16	11	1332			
			E14.5	WT	d	17	2	269		
						18	2	274		
						19	4	525		
						20	2	275		
			E18.4	WT	e	21	1	129		
						22	2	220		
		23				5	546			
		6 days	WT	f	24	4	396			
					25	4	440			
					4-6 weeks	Pou2f3 Control	g	26	4	339
						Pou2f3 KO	h	27	1	112
		CD45 <sup>+</sup> EpCAM <sup>+</sup> Sox9-eGFP <sup>+</sup>	4-6 weeks	Sox9 <sup>Cre</sup> GFP	i	28	11	549		
						29	6	572		
	Intestine	EpCAM <sup>+</sup> Hpgds-tdTomato <sup>+</sup>	4-6 weeks	Hpgds <sup>Cre</sup> tdTomato	j	30	2	376		
31						4	928			
Thymus	CD45 <sup>+</sup> IL-25R <sup>+</sup>	4-6 weeks	WT	k	32	4	951			
					33	4	1075			
					34	6	1560			
			Pou2f3 Control	l	35	4	865			
					36	2	613			
					37	2	217			
			Pou2f3 KO	m	38	2	541			
					39	2	480			
					40	2	333			
Total					135	17654				

**Extended Data Fig. 1 | Single-cell data quality controls.** **a**, Summary of all single cells analysed in this study, divided into experimental procedures. 'nbatches' indicates number of technical replicates; 'ncells' indicates number of cells after filtering (see Methods). **b–e**, Colour-coded tracks summarizing the number of Illumina reads per cell (**b**), transcripts (UMI)

detected in each cell (**c**), fraction of analysed cells from each amplification batch (**d**) and estimation of technical noise for each amplification batch (**e**). Cells are coloured by experimental procedure. Technical noise is assessed by genomic UMIs in empty wells as previously described<sup>4</sup> (see Methods).

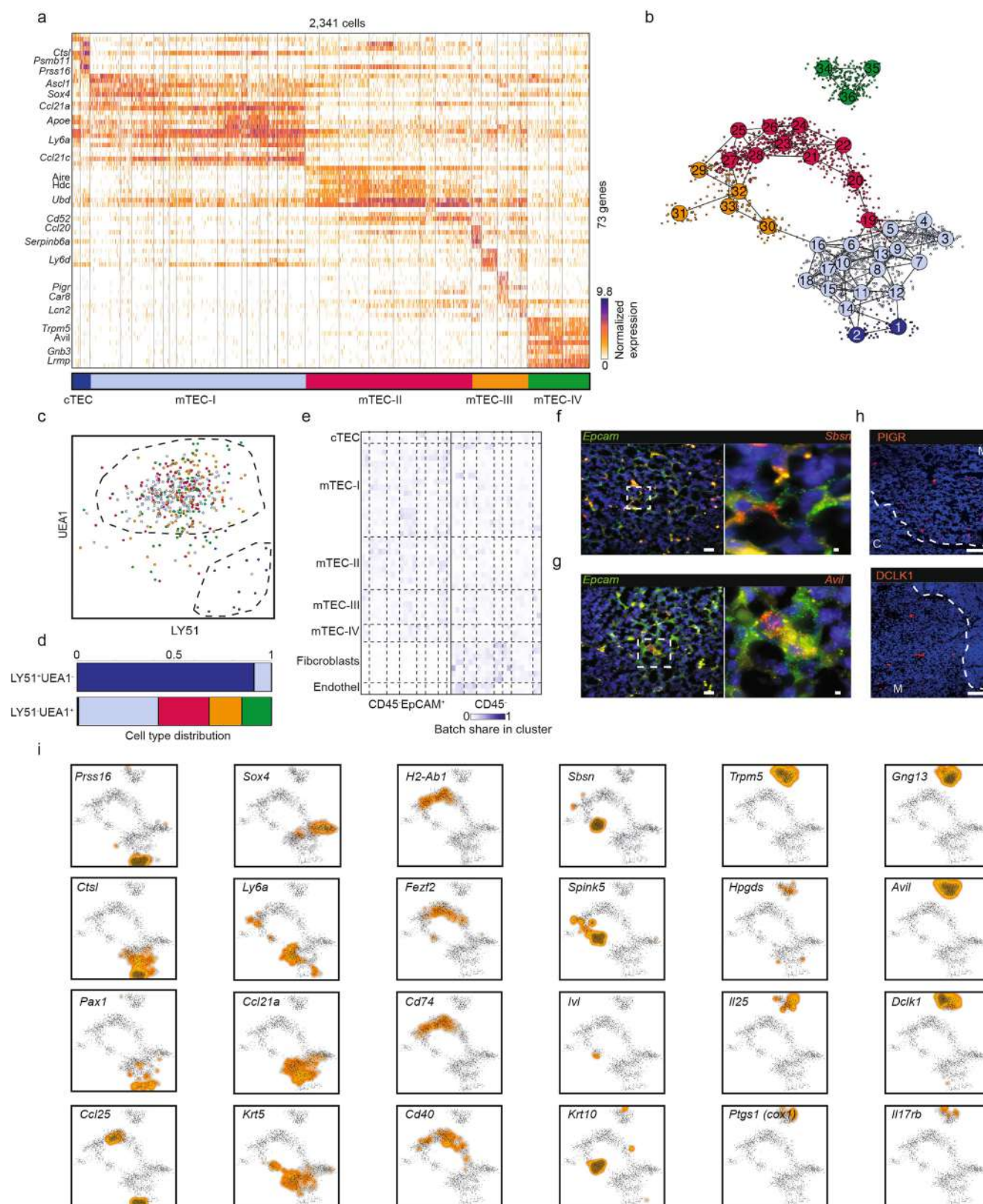




**Extended Data Fig. 2 | Thymic stroma sorting and clustering.** **a**, Flow cytometry schematic of thymic cells showing isolation of stroma cells, as well as staining for known populations markers. Immune cells, CD45; fibroblast, CD34; endothelial, CD31; mTEC, UEA1; cTEC, LY51; mature mTEC, MHC-II. The red border marks stroma single-cell sorting gate. **b**, Index sort tracks showing the intensity of protein levels for MHC-II, UEA1 and LY51 in individual single cells shown in Fig. 1a–c. **c**, Cell–cell correlation of CD45<sup>+</sup> thymic stroma cells calculated over 132 differentially

expressed genes. **d**, Pairwise distance distribution between cells within the three main stromal lineages. Distance is defined as  $1 - \text{Spearman}$ . Box plots display median bar, first-third quantile box and 5th–95th percentile whiskers.  $n = 1,825$  single cells. **e**, **f**, Gene expression profiles of 723 cells from fibroblast clusters of the CD45<sup>+</sup> stroma, marked by increased expression of *Col1a1* (**e**, Supplementary Table 1) and 221 cells from the endothelial clusters of the CD45<sup>+</sup> stroma, marked by increased expression of *Pecam1* (**f**, Supplementary Table 1).



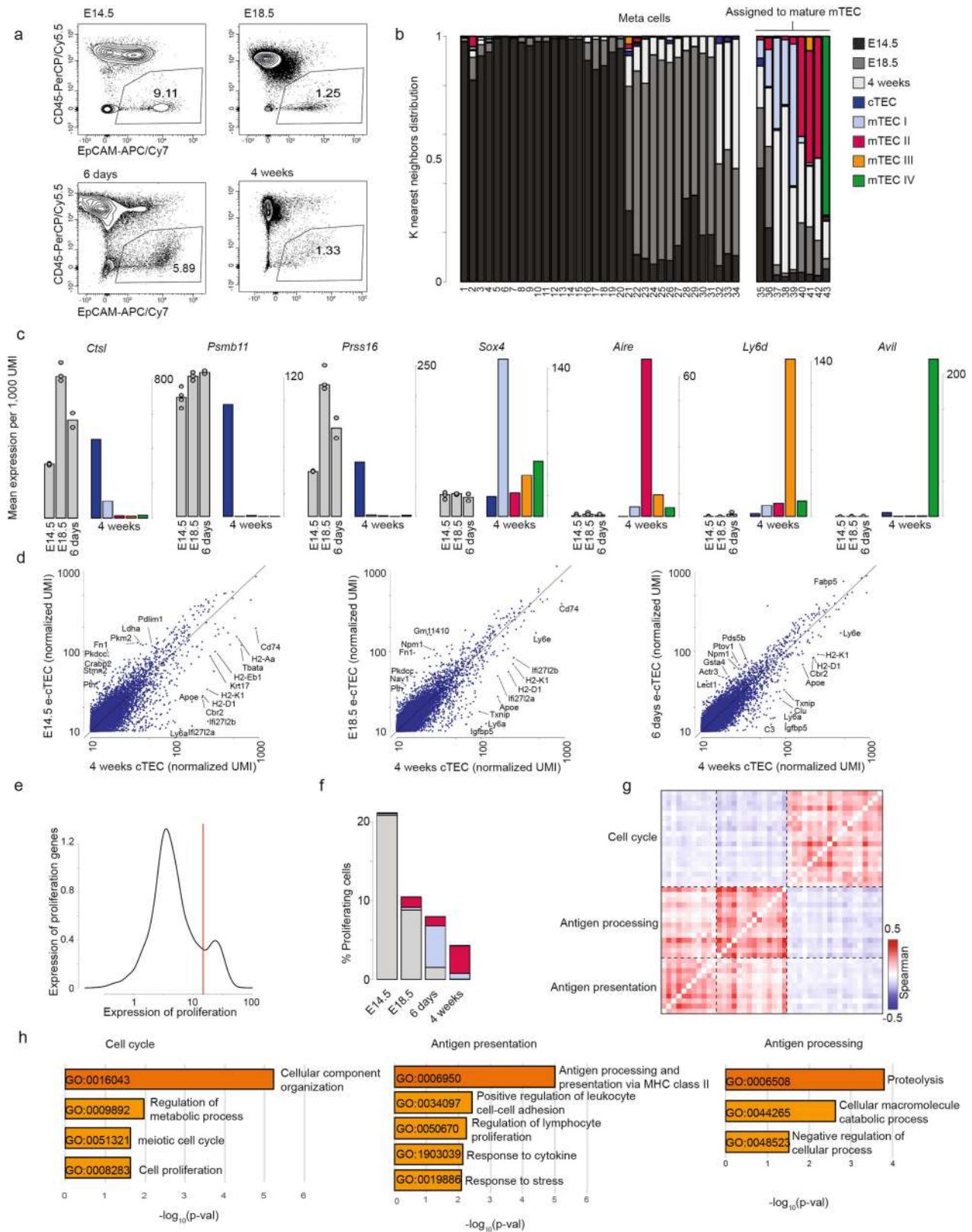


Extended Data Fig. 3 | See next page for caption.



**Extended Data Fig. 3 | Thymic epithelial cells are characterized by four subsets of mTEC and a single cTEC subset.** **a**, Heat map showing a metacell analysis of 2,341 thymic epithelial cells ( $CD45^-EpCAM^+$ ), featuring the 73 most variable genes, from 15 biological replicates of 4–6-week-old mice. Colour bar represents separation of 36 metacells into five main populations. **b**, Two-dimensional graph representation of the metacell model in Fig. 1a (see Methods). Big circles represent metacells, and are colour-coded as shown in **a**. **c**, FACS index sorting measurement of LY51 and UEA1 in epithelial cells. Cells are coloured based on cluster association as determined in **a**. Dashed lines outline  $LY51^+UEA1^-$  and  $LY51^-UEA1^+$  gates. **d**, Fraction of TEC subsets out of  $LY51^+UEA1^-$  and  $LY51^-UEA1^+$  populations, assessed by gating single cells on index sorting protein measurements of UEA1 and LY51 in **c**. **e**, Controlling for batch

effect as determined by the relative share of each batch in all metacells. Batches are ordered by biological replicate (marked by dashed lines) and sorting scheme (either  $CD45^-$  or  $CD45^-EpCAM^+$ ). **f**, **g**, Single molecule FISH assay on 5–8- $\mu m$ -thick cryosections (see Methods) using fluorescent probes against the genes *Epcam* and *Sbsn* (**f**) or *Avil* (**g**). Blue, DAPI. The experiments were repeated independently four times with similar results. **h**, Immunofluorescence images of the protein markers: PIGR and DCLK1. Medulla (M) and cortex (C) are separated by dashed lines, distinguished by nuclei density. Blue, DAPI. **f–h**, Scale bars, 20  $\mu m$ . The experiments were repeated independently twice with similar results. **i**, Projection of representative differentially expressed genes onto the two-dimensional graph of epithelial cells.



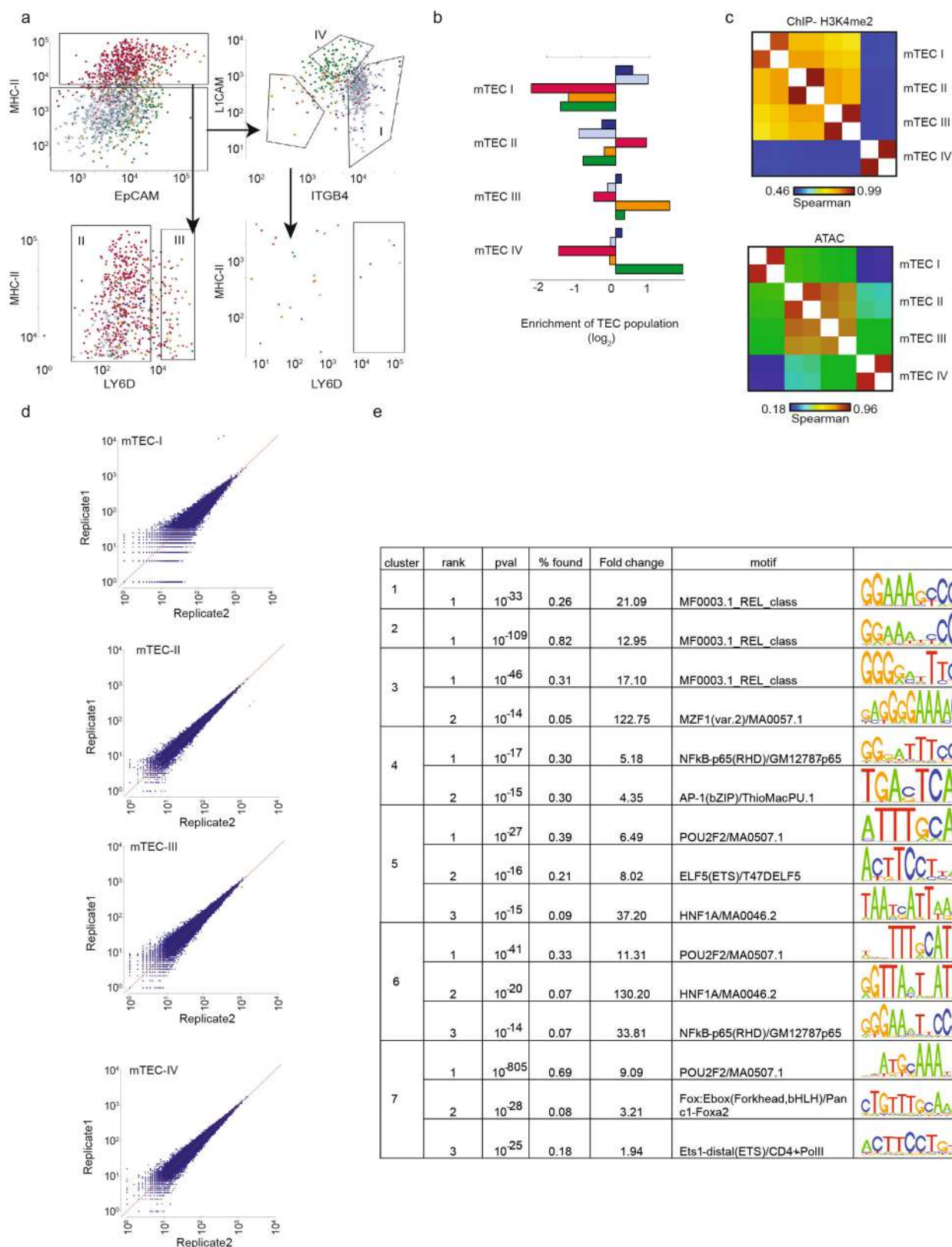
Extended Data Fig. 4 | See next page for caption.

**Extended Data Fig. 4 | TEC dynamics during thymus development.**

**a**, Flow cytometry scheme of thymic epithelial cells from different development time points. Numbers indicate fraction of  $CD45^{-}EpCAM^{+}$  cells. **b**, Summary of the  $K$  ( $K = 50$ ) nearest neighbours of embryonic cells, grouped into metacells. Neighbours of adult origin are coloured by TEC subsets, and of embryonic origin are coloured by developmental time point. Metacells with more than 20% adult neighbours were assigned to a TEC subset. **c**, Normalized mean expression of differential genes across TEC mature populations (4 weeks old) and unassigned cells from developmental time points (grey).  $n = 4$  (E14.5), 3 (E18.5) and 2 (6 days) independent animals. Data are median (bars) and individual animals (dots). **d**, Differential gene expression between early cTEC (e-cTEC) from

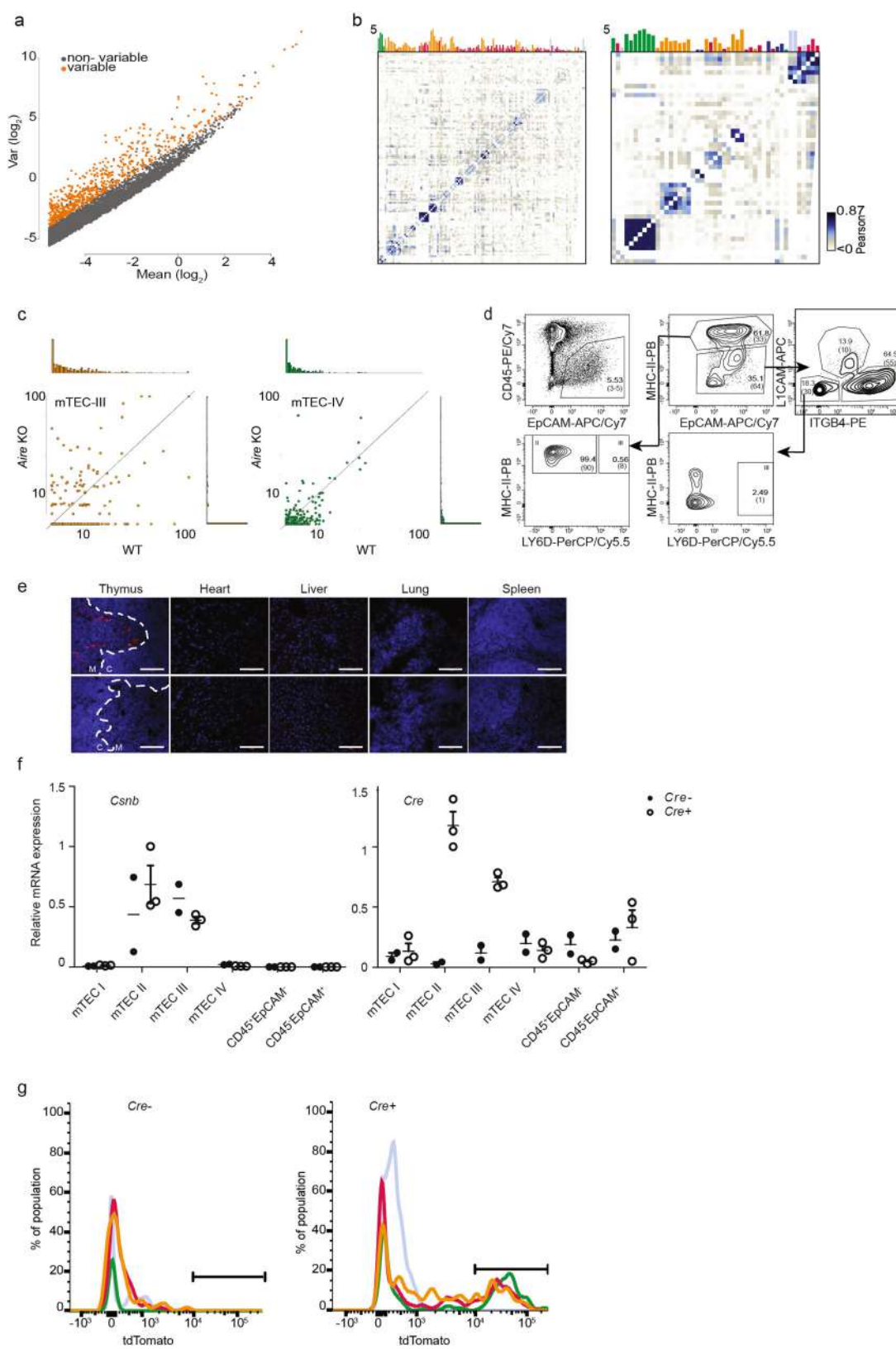
three developmental time points and the mature cTEC. Axes represent UMI count per 1,000 UMI, normalized to cell numbers. **e**, Distribution of cell cycle gene expression across cells from developing TEC is bimodal. The red line indicates the empirical proliferation threshold. **f**, Frequency of proliferating cells in the epithelial population at each developmental time point. Colour code as in **b**. **g**, Gene pairwise Spearman correlation over 2,319 e-cTEC single cells reveals three gene modules jointly expressed across embryonic early TEC and mature cTEC populations. **h**, GO annotations enrichment analysis of the three cTEC gene modules. For cell cycle,  $n = 114$ ; antigen presentation,  $n = 33$ ; and antigen processing,  $n = 56$ .





**Extended Data Fig. 5 | Genetic and epigenetic characterization of TEC subsets.** **a**, In silico gating of mTEC I–IV populations by index sorting measurements of surface markers. The same gating schemes were used to purify these populations by FACS (Fig. 2a). Cells are colour-coded as shown in Fig. 1. Blue, cTEC; light blue, mTEC I; red, mTEC II; yellow, mTEC III; green, mTEC IV. **b**, Relative enrichment ( $\log_2$  fold change compared to total  $CD45^+EpCAM^+$  epithelial cells) of the individual mTEC I–IV subsets gated according to **a**. **c**, Heat map showing pairwise Spearman

correlation of 29,472 H3K4me2 peaks (top) or ATAC-seq peaks (bottom) from mTEC I–IV sorted populations. Biological replicates for each population are shown. **d**, Scatter plots of mTEC I–IV H3K4me2 ChIP-seq peaks in biological duplicates. **e**, Summary of the most significant motifs enriched in each cluster of mTEC I–IV H3K4me2 differential peaks (Fig. 2e). *P* values are derived from binomial tests after FDR correction for multiple hypotheses. *n* = 2,302 differential peaks.

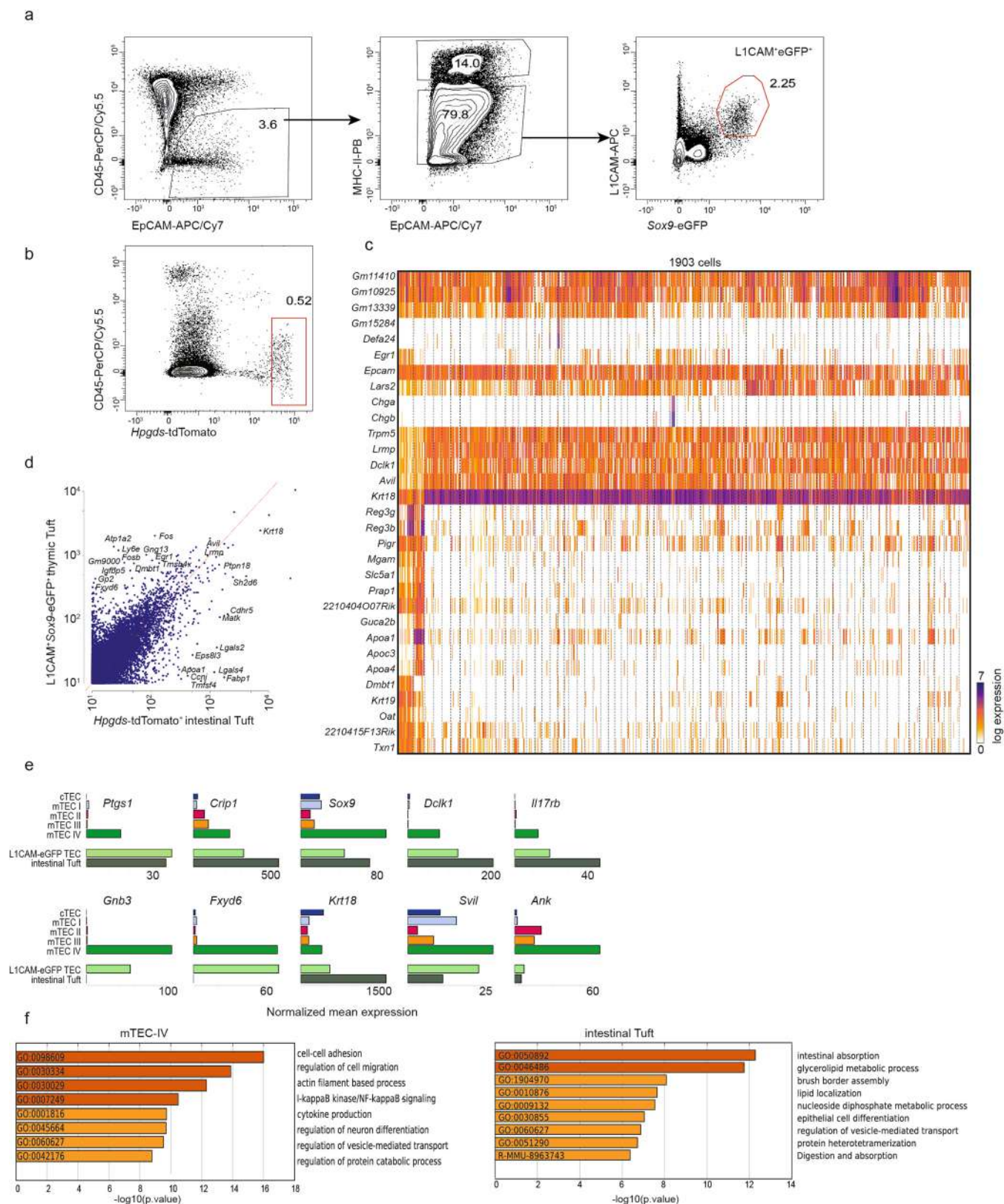


Extended Data Fig. 6 | See next page for caption

**Extended Data Fig. 6 | Characterization of AIRE-dependent mTEC subsets.** **a**, Variance of genes plotted against their mean value (genes with >50 total UMI are shown). Orange dots indicate variable genes. **b**, Pairwise Pearson gene correlations in AIRE-dependent (left) and AIRE-independent (right) TRA gene lists across 2,341 TEC single cells. Levels of differential expression (highest change of expression in cluster compared to median across all clusters) are indicated as bars; bar colours indicate cluster association to TEC population. **c**, Comparison of stochastic gene expression between *Aire* knockout and wild-type cells in mTEC III and IV populations. Marginal distribution is shown as histogram. Axes represent UMI count per 1,000 UMI, normalized to cell numbers. **d**, Flow cytometry scheme of thymic *Aire* knockout cells

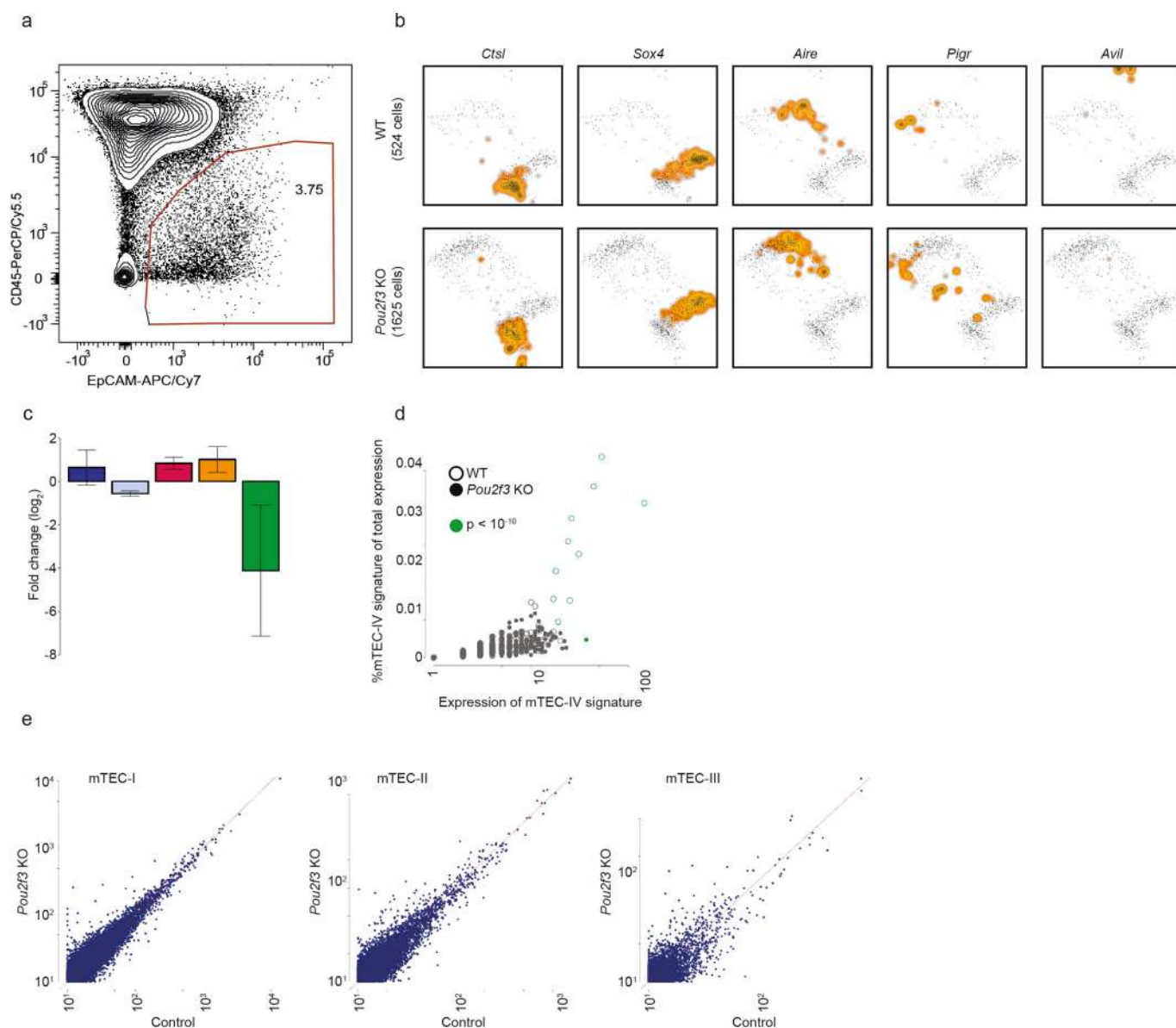
showing the percentage of each TEC population compared to wild-type percentage (shown in brackets). **e**, Representative immunofluorescence images of two independent experiments, for tdTomato across different organs. In the thymus, the medulla (M) and cortex (C) are separated by dashed lines, distinguished by nuclei density. Blue, DAPI. Scale bars, 100  $\mu$ m. **f**, qPCR analysis of *Csnb* (left) and *cre* (right) genes in *Csnb<sup>cre+</sup>Rosa26<sup>tdTomato</sup> (cre<sup>+</sup>)* and *Csnb<sup>cre-</sup>Rosa26<sup>tdTomato</sup> (cre<sup>-</sup>)* across thymic populations. Dot plots display mean and error bars indicate s.e.m.  $n = 2$  (wild type) or  $n = 3$  (*Csnb<sup>cre+</sup>*) biologically independent animals. **g**, Flow cytometric analysis of tdTomato expression in mTEC subsets (colours as in Fig. 1) isolated from thymi of *Csnb<sup>cre+</sup>Rosa26<sup>tdTomato</sup>-* or *Csnb<sup>cre-</sup>Rosa26<sup>tdTomato</sup>-reporter* mice.





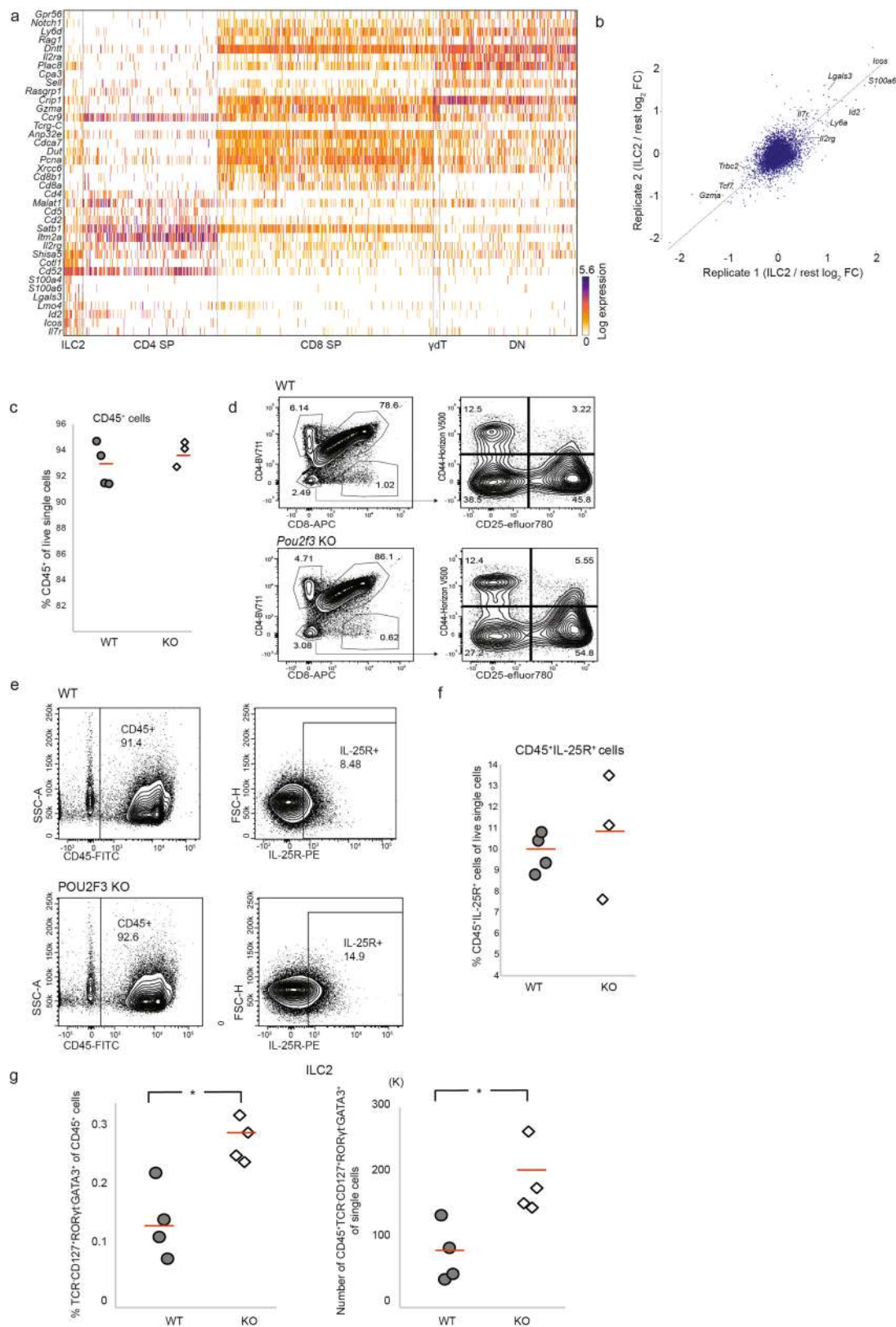
**Extended Data Fig. 7 | Comparing intestinal tuft cells and the mTEC IV population.** **a**, Flow cytometry scheme of mTEC IV cells ( $Sox9$ -eGFP<sup>+</sup>L1CAM<sup>+</sup>) sorting. **b**, Flow cytometry scheme of small intestine  $Hpgds$ -tdTomato<sup>+</sup> tuft cell sorting. **c**, Heat map showing gene expression profiles across 1,903 intestinal tuft ( $Hpgds$ -tdTomato<sup>+</sup>) single cells, grouped into 68 metacells. **d**, Comparison of gene expression between tuft cells isolated from small intestine ( $Hpgds$ -tdTomato<sup>+</sup>; x axis) and mTEC

IV cells isolated from thymus ( $CD45$ -EpCAM<sup>+</sup> $Sox9$ -eGFP<sup>+</sup>L1CAM<sup>+</sup>; y axis). Axes represent UMI count per 1,000 UMI, normalized to cell numbers. **e**, Normalized mean expression of differential genes across TEC populations, sorted mTEC IV cells (L1CAM<sup>+</sup> $Sox9$ -eGFP<sup>+</sup>) and intestinal Tuft ( $Hpgds$ -tdTomato<sup>+</sup>) cells. **f**, GO annotations enrichment in differential genes (fold change >2) between intestinal tufts ( $n = 634$ ) and mTEC IV cells (L1CAM<sup>+</sup> $Sox9$ -eGFP<sup>+</sup>) ( $n = 1,308$ ).



**Extended Data Fig. 8 | The transcription factor *Pou2f3* is a master regulator of mTEC IV.** **a**, Flow cytometry scheme for sorting of EpCAM<sup>+</sup> cells from *Pou2f3* knockout thymi. **b**, Projection of representative TEC subtype-specific markers onto the two-dimensional mapping of *Pou2f3* wild-type and knockout cells to the epithelial model of Fig. 1 (see Methods). **c**, Bar plot showing  $\log_2$  fold change between TEC subpopulation abundances in *Pou2f3* knockout ( $n = 451$  single cells) and wild-type ( $n = 1121$ ) mice. Error bars represent 95% confidence intervals.

**d**, Pooled expression of mTEC IV genes across cells from *Pou2f3* knockout and wild-type (WT) mice. The  $x$  axis represents UMI count per 1,000 UMI;  $y$  axis represents fraction of expression from total UMI count of the cells. Green cells indicate cells classified as mTEC IV (two-sided binomial test; FDR-adjusted  $P < 10^{-10}$ ).  $n = 1,572$  single cells. **e**, Differential gene expression between mTEC I–III cells isolated from control (wild-type) and *Pou2f3* knockout mice. Axes represent UMI count per 1,000 UMI, normalized to cell numbers.



### Extended Data Fig. 9 | mTEC IV shape the thymus immune niche.

**a**, Heat map showing a metacell analysis of 3,500 CD45<sup>+</sup>IL-25R<sup>+</sup> cells across five clusters. **b**, Differential gene expression in ILC2 cells from two biological replicates compared to other CD45<sup>+</sup>IL-25R<sup>+</sup> cells (rest) from each replicate. Axes represent log<sub>2</sub> fold change. **c**, Percentages of CD45<sup>+</sup> cells in *Pou2f3* knockout and wild-type thymi, determined by flow cytometry. Circles and diamonds indicate independent mice, centre line indicates the mean value. **d**, Flow cytometry analysis of cells expressing CD4, CD8, CD25 and CD44 in *Pou2f3* knockout and wild-type thymi. The experiment was repeated independently four times with

similar results to confirm reproducibility. **e**, Flow cytometry sorting scheme of thymic CD45<sup>+</sup>IL-25R<sup>+</sup> cells from *Pou2f3* knockout and wild-type thymi. **f**, Percentage of CD45<sup>+</sup>IL-25R<sup>+</sup> cells in *Pou2f3* knockout and wild-type thymi. Circles and diamonds indicate independent mice, centre line indicates the mean value. **g**, Percentages (left) and numbers (right) of ILC2 (Lin<sup>+</sup>TCR<sup>+</sup>CD127<sup>+</sup>GATA3<sup>+</sup>Rorγt<sup>+</sup>) cells within the single-cell gate in *Pou2f3* knockout and wild-type mice. Circles and diamonds indicate independent mice, centre line indicates the mean value. A one-tailed Student's *t*-test was used for the comparison, \**P* < 0.05.



**Extended Data Table 1 | Regions of enhancer enrichment peaks****a.**

Sample	Replicate	number of iChIP aligned reads	number of IDR peaks
mTEC-I	a	13831980	7037
mTEC-I	b	3359743	
mTEC-II	a	32464771	23950
mTEC-II	b	29099226	
mTEC-III	a	17032161	19322
mTEC-III	b	17710805	
mTEC-IV	a	18818509	22758
mTEC-IV	b	17910967	

**b.**

Sample	Replicate	number of ATAC aligned reads	Number of peaks
mTEC-I	a	12521131	44288
mTEC-I	b	10665995	39040
mTEC-II	a	6626821	19008
mTEC-II	b	8633041	27739
mTEC-III	a	10899189	10525
mTEC-III	b	2387938	19507
mTEC-IV	a	8388701	30017
mTEC-IV	b	13972276	38108

**a.** H3K4me2 iChIP-seq peak calling. **b.** ATAC-seq peak calling.



## Reporting Summary

Nature Research wishes to improve the reproducibility of the work that we publish. This form provides structure for consistency and transparency in reporting. For further information on Nature Research policies, see [Authors & Referees](#) and the [Editorial Policy Checklist](#).

### Statistical parameters

When statistical analyses are reported, confirm that the following items are present in the relevant location (e.g. figure legend, table legend, main text, or Methods section).

n/a Confirmed

- ☐ ☒ The exact sample size (*n*) for each experimental group/condition, given as a discrete number and unit of measurement
- ☐ ☒ An indication of whether measurements were taken from distinct samples or whether the same sample was measured repeatedly
- ☐ ☒ The statistical test(s) used AND whether they are one- or two-sided  
*Only common tests should be described solely by name; describe more complex techniques in the Methods section.*
- ☒ ☐ A description of all covariates tested
- ☐ ☒ A description of any assumptions or corrections, such as tests of normality and adjustment for multiple comparisons
- ☐ ☒ A full description of the statistics including central tendency (e.g. means) or other basic estimates (e.g. regression coefficient) AND variation (e.g. standard deviation) or associated estimates of uncertainty (e.g. confidence intervals)
- ☐ ☒ For null hypothesis testing, the test statistic (e.g. *F*, *t*, *r*) with confidence intervals, effect sizes, degrees of freedom and *P* value noted  
*Give P values as exact values whenever suitable.*
- ☒ ☐ For Bayesian analysis, information on the choice of priors and Markov chain Monte Carlo settings
- ☒ ☐ For hierarchical and complex designs, identification of the appropriate level for tests and full reporting of outcomes
- ☐ ☒ Estimates of effect sizes (e.g. Cohen's *d*, Pearson's *r*), indicating how they were calculated
- ☐ ☒ Clearly defined error bars  
*State explicitly what error bars represent (e.g. SD, SE, CI)*

Our web collection on [statistics for biologists](#) may be useful.

### Software and code

Policy information about [availability of computer code](#)

Data collection

Microscope softwares: MetaMorph 7.8.2.0, NIS element 4.13.05. Flow cytometry software: Diva7.

Data analysis

ChIP and ATAC data analysis, including motif finding was done with the HOMER 4.8 package.  
Single cell data was analyzed with the MetaCell package, which is available upon request.  
Fiji ImageJ 1.5 software was used to analyze microscope data.  
HISAT 0.1.6 was used for reads mapping.  
Metascape software was used for genes annotation and enrichment analysis.

For manuscripts utilizing custom algorithms or software that are central to the research but not yet described in published literature, software must be made available to editors/reviewers upon request. We strongly encourage code deposition in a community repository (e.g. GitHub). See the Nature Research [guidelines for submitting code & software](#) for further information.

## Data

Policy information about [availability of data](#)

All manuscripts must include a [data availability statement](#). This statement should provide the following information, where applicable:

- Accession codes, unique identifiers, or web links for publicly available datasets
- A list of figures that have associated raw data
- A description of any restrictions on data availability

Genomic data available in GEO dataset numbers: GSE103967, GSE103968, GSE103969, GSE103970.

## Field-specific reporting

Please select the best fit for your research. If you are not sure, read the appropriate sections before making your selection.

☒ Life sciences ☐ Behavioural & social sciences ☐ Ecological, evolutionary & environmental sciences

For a reference copy of the document with all sections, see [nature.com/authors/policies/ReportingSummary-flat.pdf](https://www.nature.com/authors/policies/ReportingSummary-flat.pdf)

## Life sciences study design

All studies must disclose on these points even when the disclosure is negative.

Sample size	No statistical methods were used to predetermine sample size. Sample sizes for animal studies were made as large as possible based on the complex genetics. Number of sequenced single cells (13,000) was determined to ensure detection of subpopulations and is on par with technical standards in the field.
Data exclusions	See Methods "clustering" section. Cells with less than 500 UMIs were excluded.
Replication	All samples were done in biological and technical replicates as is reported in extended data Fig. 1. All experiments were replicated at least two times. All replications yielded similar results. The main reconstruction of the thymic stromal populations was based on at least seven independent animals
Randomization	No randomization was done, since all animals used were isogenic mice. Human samples were taken from cardiac surgery patients without randomization
Blinding	No blinding was done, since the computational framework was identical for all processed animal samples.

## Reporting for specific materials, systems and methods

### Materials & experimental systems

n/a	Involved in the study
<input checked="" type="checkbox"/>	<input type="checkbox"/> Unique biological materials
<input type="checkbox"/>	<input checked="" type="checkbox"/> Antibodies
<input checked="" type="checkbox"/>	<input type="checkbox"/> Eukaryotic cell lines
<input checked="" type="checkbox"/>	<input type="checkbox"/> Palaeontology
<input type="checkbox"/>	<input checked="" type="checkbox"/> Animals and other organisms
<input type="checkbox"/>	<input checked="" type="checkbox"/> Human research participants

### Methods

n/a	Involved in the study
<input type="checkbox"/>	<input checked="" type="checkbox"/> ChIP-seq
<input type="checkbox"/>	<input checked="" type="checkbox"/> Flow cytometry
<input checked="" type="checkbox"/>	<input type="checkbox"/> MRI-based neuroimaging

## Antibodies

### Antibodies used

Antibodies for flow cytometry analysis:

APC-Cy7-EpCAM (118218); PE-Ly51 (108308); Pacific-Blue-I-A/I-E (107620); PerCP Cy5.5-CD45 (103132); FITC-CD34 (343603); APC-CD31 (102409); PE-Cy7-CD45 (103114); FITC-Itgb4 (123605); PE-Itgb4 (123610); PE-IL17RB (IL25R,146305) were purchased from Biolegend; APC-L1CAM (FAB5674R) was purchased from Novus; APC-Gata3 (560078); Brilliant Violet 650-Rorgt (564722); biotinylated-CD3 (553060); biotinylated-CD4 (553728); biotinylated-CD8 (553029); biotinylated-B220 (553086); biotinylated-Ter119 (553672); biotinylated-CD11c (553800); biotinylated-Gr1 (553125); FITC-CD45 (553080); FITC-CD8 (553031); APC-Ter119 (557909); PE-Cy7-CD45 (552848); BV711-CD4 (563726); APC-CD8 (553035); Horizon V500-CD44 (560780) were purchased from BD; and PerCP-e710-Ly-6d (4330516); PE-Cy7 CD127 (25-1273-82); PE-Tbet (12-5825-82); eFluor780-CD4 (47-0042-82);

eFluor780-CD25 (47-025182) were purchased from eBioscience. In addition, the following materials were also used for FACS staining: 7-AAD Viability Staining Solution (Biolegend, 420404); Biotinylated Ulex Europaeus Agglutinin I (UEA I) (Vector laboratories, B-1065), PE-cy7-Streptavidin, PerCP-Cy5.5-Streptavidin (554064, BD), SYTOX (S34857; Invitrogen), FcR blocker (BE0307; Bio X cell).

Antibodies for Immunofluorescence:

PE anti-Ly51 (108308; Biolegend), Anti-DCLK1 (ab37994; Abcam); APC anti Itga6 (313615; Biolegend); anti-villin (MAB1671; Millipore); Anti-COX1 (sc-1754; Santa Cruz Biotechnology); Anti-DCLK1 (ab37994; Abcam), Anti Psmb11 (pd021, MBL), anti PigR (AF2800, R&Dsystems). Goat anti Rabbit AF555, Jackson, Purified Rat Anti-Mouse CD16/CD32 (Bio X cell, BE0307, or Biolegend, 101302).

Antibody for ChIP experiment:

Anti H3K4me2 (abcam; ab3254)

Validation

Antibodies were validated in the companies from which they were purchased.

## Animals and other organisms

Policy information about [studies involving animals](#); [ARRIVE guidelines](#) recommended for reporting animal research

Laboratory animals

4-9 weeks old female CBL57/6 mice were used in this study.

Wild animals

No wild animals were used.

Field-collected samples

No field collected samples were used.

## Human research participants

Policy information about [studies involving human research participants](#)

Population characteristics

8 days to 9 years old male human thymic samples were obtained in the course of corrective cardiac surgery at Schneider Children's Medical Center of Israel.

Recruitment

Cardiac surgery patients were recruited tentatively pre-cardiac surgery, so in case of thymus removal, the sample will be donated to the experiment. No bias of self selection is relevant.

## ChIP-seq

### Data deposition

☒ Confirm that both raw and final processed data have been deposited in a public database such as [GEO](#).

☒ Confirm that you have deposited or provided access to graph files (e.g. BED files) for the called peaks.

Data access links

*May remain private before publication.*

GSE103967-GSE103970

Files in database submission

H3K4me2-TEC-cluster-1-3-A\_S112.R1.fastq.gz  
H3K4me2-TEC-cluster-1-3-A\_S112.R2.fastq.gz  
H3K4me2-TEC-cluster-1-3-B\_S117.R1.fastq.gz  
H3K4me2-TEC-cluster-1-3-B\_S117.R2.fastq.gz  
H3K4me2-TEC-cluster-5-6-A\_S114.R1.fastq.gz  
H3K4me2-TEC-cluster-5-6-A\_S114.R2.fastq.gz  
H3K4me2-TEC-cluster-5-6-B\_S119.R1.fastq.gz  
H3K4me2-TEC-cluster-5-6-B\_S119.R2.fastq.gz  
H3K4me2-TEC-cluster-7-10-A\_S115.R1.fastq.gz  
H3K4me2-TEC-cluster-7-10-A\_S115.R2.fastq.gz  
H3K4me2-TEC-cluster-7-10-B\_S120.R1.fastq.gz  
H3K4me2-TEC-cluster-7-10-B\_S120.R2.fastq.gz  
H3K4me2-TEC-cluster-12-A\_S116.R1.fastq.gz  
H3K4me2-TEC-cluster-12-A\_S116.R2.fastq.gz  
H3K4me2-TEC-cluster-12-B\_S121.R1.fastq.gz  
H3K4me2-TEC-cluster-12-B\_S121.R2.fastq.gz  
H3K4me2-TEC-cluster-1-3-Combined\_peaks-top-set.txt  
H3K4me2-TEC-cluster-5-6-Combined\_peaks-top-set.txt  
H3K4me2-TEC-cluster-7-10-Combined\_peaks-top-set.txt  
H3K4me2-TEC-cluster-12-Combined\_peaks-top-set.txt  
H3K4me2-TEC-cluster\_IDR\_merged\_annotated\_iChIP\_peaks\_counts.txt

Genome browser session  
(e.g. [UCSC](#))

Provide a link to an anonymized genome browser session for "Initial submission" and "Revised version" documents only, to enable peer review. Write "no longer applicable" for "Final submission" documents.

## Methodology

Replicates	Two biological replicates for each sample Whole cell extract without antibodies as control.
Sequencing depth	Mean of 10M reads for a sample
Antibodies	H3K4me2- abcam ab3254
Peak calling parameters	findPeaks <input tag directory> -o <out file> -style histone -i <WCE tag directory>
Data quality	IDR using from Qunhua Li and Anshul Kundaje method (Oct,2010)
Software	Homer ( <a href="http://homer.ucsd.edu/homer/">http://homer.ucsd.edu/homer/</a> )

## Flow Cytometry

### Plots

Confirm that:

- ☒ The axis labels state the marker and fluorochrome used (e.g. CD4-FITC).
- ☒ The axis scales are clearly visible. Include numbers along axes only for bottom left plot of group (a 'group' is an analysis of identical markers).
- ☒ All plots are contour plots with outliers or pseudocolor plots.
- ☒ A numerical value for number of cells or percentage (with statistics) is provided.

### Methodology

Sample preparation	<p>Preparation of thymi for TEC- Murine thymi were treated with enzymes cocktail (Collagenase, Dispase and Dnase) at 37C. Cells were separated by Percoll gradient density centrifugation, filtered and stained with Flow cytometry antibodies.</p> <p>Preparation of thymi for hematopoietic cells- Murine thymi weresmashed through 40um cell strainer, washed, filtered and stained with Flow cytometry antibodies. When needed, fixation and permeabilization were done, followed by staining with intracellular markers antibodies.</p> <p>Preparation of intestine- murin small intestines were flushed with PBS, treated with EDTA, Dispase and Dnase, filtered and stained with Flow cytometry antibodies.</p>
Instrument	BD FACSAria Special Order Research Product (SORP) or BD FACSAria Fusion or BD FACSAriaIII or BD FACS Cantoll
Software	Data collection was done using FACS Diva 7, data analysis was done using FlowJo software (Tree Star Inc.).
Cell population abundance	We assessed the abundance of the relevant cell population based on in-silico gating of index-sorted single cells with the relevant markers.
Gating strategy	Pre gating was first done for live cells based on 7-AAD/SYTOX/DAPI stain, followed by single cells gating according to their pattern in the FSC-A vs. FSC-W and FSC-A vs. SSC-A plots, then gating was performed using specific markers antibodies, as shown in figures and methods.

- ☒ Tick this box to confirm that a figure exemplifying the gating strategy is provided in the Supplementary Information.